NJC

ROYAL SOCIETY OF CHEMISTRY

PERSPECTIVE

Cite this: *New J. Chem.*, 2022, **46**, 7309

Recent advances in tin ion detection using fluorometric and colorimetric chemosensors

Saikat Kumar Manna, *[a] Sanchita Mondal, *[b] Barnali Jana[a] and Khokan Samanta[a]

Received 23rd January 2022,
Accepted 16th March 2022

DOI: 10.1039/d2nj00383j

rsc.li/njc

The innovation of chemosensors for tin ions (Sn^{4+}/Sn^{2+}) has evolved as a key research topic in recent decades, garnering a lot of attention due to their environmental, industrial and biological importance. In recent years, there has been a significant amount of research on tin ion chemosensors. This review will concentrate on the development of tin ion chemosensors from 2012 to 2022, with Sn^{4+} and Sn^{2+} being discussed individually. In addition, the comparison data of all of these probes have been presented, as well as the future opportunities and current issues, in this review. As far as we know, this is the first review of tin chemosensors.

1. Introduction

Tin (Sn) is a vital trace mineral for human and animal life, with both positive and negative effects, and is commonly found at low concentrations in the environment.[1,2] Tin has two oxidation states, +4 (stannic) and +2 (stannous), both of which are quite stable and may be interconverted with relatively active reagents. Tin is found at the highest concentrations in the adrenal glands, thyroid gland, liver, brain, and spleen.[3–6] It plays a variety of roles in the human body, including cancer prevention, human growth factors, and a variety of biological processes.[7–9] However, in humans, a lack of tin can create issues such as hearing loss, respiratory problems, decreased production of haemoglobin and DNA damage.[10–13] But, due to excessive accumulation, it has certain negative impacts on human health and the environment. Tin (Sn), a heavy metal that is present in water, air, and soil, is widely employed in a variety of industries, including food processing equipment, food containers, toothpastes, soaps, perfumes, dyes, food additives, antifouling paints, biocides, PVC stabilizers, tin plates, jewelry models, packaged foods, and mouthwashes.[14,15] Tin is also utilised in the manufacturing of biodiesel, the allylation of carbonyl compounds, and the preparation of PGF derivatives, graphene sheets, and indole and coumarin derivatives.[16–21] Besides, tin may produce organotin by forming covalent bonds with carbon. Although tin can appear in either the Sn^{2+} or Sn^{4+} oxidation state, practically all organotins have a tetravalent structure. Organotin compounds (OTC) are utilised in the manufacture of insecticides, disinfectants, polyurethane foams, pest repellents, paints, plastics and PVC stabilisers.[22–25] Since the 1950s, Sn(II) salts have been used in dentistry as a chemical adjuvant to prevent tooth cavities.[26] Furthermore, it was observed that Sn(II) salts effectively suppress *Streptococcus mutans*, which cause tooth decay in human interproximal dental plaque and oral infections.[27,28] Surprisingly, Sn(II) salts are also used in the production of many technetium-99m (^{99m}Tc) labelled radiopharmaceuticals in nuclear medicine, as well as the synthesis of polylactic acid.[29–31] Despite its significant role, excessive tin accumulation can result in gastrointestinal complaints (like nausea, abdominal cramps, and vomiting and diarrhea), immune system malfunctions, chromosomal damage, urination problems, illness and drowsiness, stomach problems, liver failure, skin and eye irritation, headaches, and breathlessness.[32–35] In 2011, Ghaffari *et al.* reported the *in vitro* impacts of numerous metals, including tin, on sperm creatine kinase and found that it lowers sperm metabolism, which is thought to be a cause of male infertility.[36] Again, tin was found to be particularly toxic to human embryonic kidney cells.[37] Many organotin compounds, such as triethyltin and trimethyltin, have been shown to be very neurotoxic.[38–40] Tributyl tin (TBT) is extremely hazardous to marine invertebrates, and its persistence in sediments raises concerns about its influence on organisms.[41] Diorganotin compounds generate cerebral oedema and restrict mitochondrial respiration by blocking keto acid oxidation, likely *via* inhibition of alpha-keto oxidase activity.[42,43] Butyltin and octyltin have been proven to have an impact on the immune system in a variety of animal species.[44,45] As a result of the risks posed by tin to humans, tin consumption must be closely monitored. Hence, the intake level of Sn is also important, and according to World Health Organization (WHO) recommendations, 8.4×10^{-4} M to 8.4×10^{-3} M and 2.105×10^{-6} M are acceptable in drinking water and canned foods, respectively.[46,47] As a result, there is a pressing need to develop sensitive, selective, effective, and affordable analytical

[a] *Department of Chemistry, Haldia Government College, Debhog, Haldia, Purba Medinipur – 721657, West Bengal, India. E-mail: saikat.manna.chem@gmail.com*
[b] *Department of Chemistry, Sree Chaitanya College, Habra, North 24 Parganas, West Bengal-743268, India. E-mail: mondalsanchita2011@gmail.com*

approaches for monitoring tin in the biological and environmental systems.

Until now, different conventional analytical techniques for identifying tin, such as atomic absorption/emission spectrometry, adsorptive stripping voltammetry, liquid chromatography, electrochemical analysis, potentiometric membrane sensing, spectrophotometry and inductively coupled plasma optical emission spectrometry (ICP OES), have been reported; however, these tools frequently require intensive and costly apparatus, rigorous sample preparation, specialised workers, and the use of hazardous solvents, rendering them impractical for real-time research.[48–58] As a result, innovative analytical devices that are environmentally sustainable, cost-effective, selective, and sensitive are required. Hence, colorimetric and fluorogenic chemosensors/chemodosimeters, *i.e.*, reaction based chemosensors,[59–65] from the spectral field are more reliable and simpler for tin ion detection than other methods due to their relatively low cost, ease, responsiveness, dependability, rapidity and specificity. These sensing methods[66–69] are highly useful for monitoring tin in a variety of biological and environmental samples (such as waste water, air, and residues). In the past few decades, many researchers have given extensive consideration to the design, synthesis, and improvement of novel colorimetric and fluorescent chemosensors for the selective and sensitive recognition of tin ions owing to their promising analytical applications.

Up to now, there are numerous published review articles on several analytes[70–75] but to the best of our knowledge, this is the first review article on chromogenic and fluorogenic tin chemosensors. In this study, we will focus on the chromogenic and fluorogenic chemosensors that have already been developed for the detection of tin ions since 2012. These sensors are categorised according to their sensing mechanism toward the different oxidation state of tin (Sn^{4+} or Sn^{2+}). The design techniques, sensing processes, and applications of several Sn^{4+}/Sn^{2+} selective chemosensors will also be reviewed. Finally, we discuss our perspectives on the generation of novel sensors for detecting tin ions in environmental and biological samples.

2. Chemosensors for tin ions

2.1. Sn^{4+} chemosensors

2.1.1. Rhodamine-based chemosensors. Rhodamine B is a well-known fluorescent dye belonging to the xanthene family, and its derivatives are commonly used as fluorescent chemosensors owing to their unique photophysical features, including high molar extinction coefficients, large fluorescence quantum yields, remarkable photostability, and long absorption and emission wavelengths.[76,77] Generally, rhodamine derivatives exist in two forms, the spirocyclic form and the ring-opened form, which have significantly distinct optical characteristics. The spirocyclic form is nonfluorescent and colourless, but it can be transformed to highly fluorescent and pink colored ring-opened form *via* coordination with some particular metal cations. This distinctive feature of rhodamine derivatives has been successfully employed for the development "off–on" chemosensors for metal ions during the past several years. In this section, we have reported 11 rhodamine-based chemosensors for Sn^{4+} ions.

In 2012, Wang *et al.* constructed a naphthalimide-rhodamine B derivative **1** for colorimetric and fluorometric sensing of Sn^{4+}, Cu^{2+} and Cr^{3+} ions.[78] Probe **1** could detect these ions (Sn^{4+}, Cu^{2+} and Cr^{3+}) with a light yellow to red absorption change (wavelength at 555 nm) within 1 min. Upon addition of these ions to probe **1** ethanol–HEPES (2 : 1, v/v) solution, the emission band underwent a red shift from 523 to 580 nm, followed by a fluorescence color change from light yellow to orange which could be seen with the naked eye. Such optical property changes were attributed to the metal induced spirolactam ring opening of probe **1** and activation of the Förster resonance energy transfer (FRET) mechanism from the naphthalimide to rhodamine unit (Fig. 1). However, upon gradual addition of EDTA to the *in situ* generated metal complex(**1**-Sn^{4+}) solution, the red color and orange fluorescent color partly turned to the original color owing to the decomplexation of Sn^{4+} ions, indicating the reversible nature of the probe for Sn^{4+} ions. In addition, probe **1** did not exhibit reversible properties for other two metal ions (Cu^{2+} and Cr^{3+} ions). The detection limit and association constant for Sn^{4+} ions were found to be 1.1×10^{-5} M and $K_a = (4.73 \pm 0.05) \times 10^3$ M^{-1}, respectively. The cell imaging capability of probe **1** for Sn^{4+} was also demonstrated in HeLa cells.

Mahapatra and co-workers developed probe **2** for the selective and sensitive detection of Sn^{4+} based on a 1 : 1 (metal : probe) binding mode with an oxo-chromene functionalized rhodamine B derivative fluorophore.[79] With the gradual addition of Sn^{4+} ions to the probe solution (CH_3OH/H_2O = 4 : 1, v/v, 10 μM HEPES buffer, pH = 7.4), the absorption band at 555 nm exhibited a noteworthy enhancement and the solution colour turned from

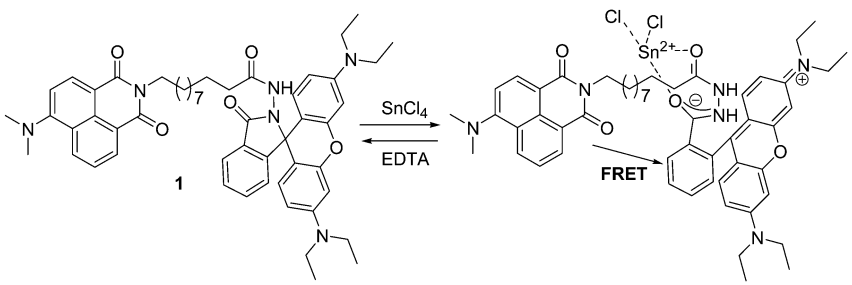

Fig. 1 Chemical structure of probe **1** and its proposed sensing mechanism.

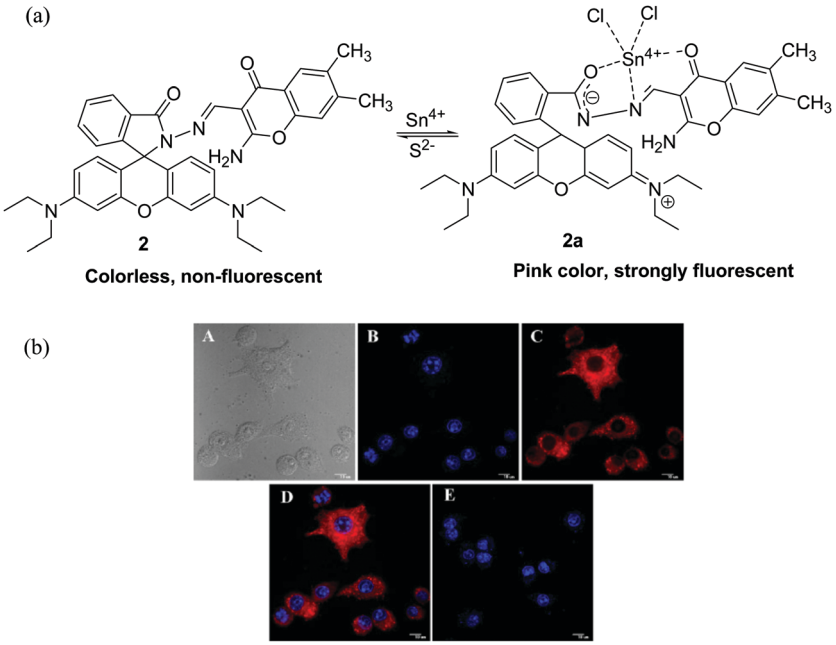

Fig. 2 (a) Chemical structure of probe **2** and its proposed sensing mechanism. (b) Confocal microscopy images of RAW 264.7 cells (A: bright field image of cells, B: only $SnCl_4$, C: $SnCl_4$+ probe, D: overlay image, E: $SnCl_4$ + probe + Na_2S). Reprinted (adapted) with permission from ref. 79. Copyright (2013) American Chemical Society.

colourless to pink. After that, the addition of 3 equivalents of Sn^{4+} ions resulted in an obvious enhancement in fluorescence (14-fold) at 580 nm and an identifiable colorimetric shift from colourless to orange. The sensing process was mainly due to the Sn^{4+} triggered transformation of the colourless and non-fluorescent spirocyclic structure (**2**) to the colored and highly fluorescent ring opened conjugated structure (**2a**), as shown in Fig. 2. From the Job's plot experiment, the stoichiometry of the complex obtained from probe **2** and Sn^{4+} was estimated to be in a ratio of 1 : 1 and the binding constant from the Benesi–Hildebrand equation was found to be as high as 4.31×10^4 M^{-1}. Moreover, the proposed binding approach was also confirmed by HRMS, FT-IR spectroscopy and DFT (density functional theory) calculations. The detection limit of **2** was calculated to be 2.58 μM based on the fluorometric titration data. In addition, the authors demonstrated that the fluorescence intensity of **2** varies in a reversible fashion in the presence of Na_2S and Na_2EDTA solutions. This probe showed high selectivity to Sn^{4+} ions without any interference from other competitive ions. Probe **2** was found to be cell permeable and effective at imaging intracellular Sn^{4+} ions in living RAW 264.7 cells during cell imaging experiments.

In 2014, the Mahapatra research group designed and synthesized a colorimetric and fluorometric chemosensor **3** for the sensing of Sn^{4+} based on the metal induced spirolactam ring opening of the rhodamine unit.[80] In aqueous ethanolic solution (HEPES, 10 mM, pH = 7.4, 1 : 4, v/v), Sn^{4+} generated a distinctive enhancement in both the fluorescence (λ_{max} = 582 nm, >2300-fold)) and absorption spectra (563 nm) of probe **3**, presenting the fluorogenic and chromogenic dual mode for Sn^{4+} detection. The probe presented an excellent linear relationship with Sn^{4+} concentrations ranging from 3.96 to 112 μM. The sensing mechanism of **3** for Sn^{4+} is shown in Fig. 3. The Job's plot demonstrated that probe **3** formed a 1 : 1 complex with the Sn^{4+} ions. Theoretical calculations, ^{1}H NMR titration, mass spectroscopy and FT-IR experiments were performed to verify the mechanism of probe **3**. The association constant was estimated to be $(1.414 \pm 0.41) \times 10^4$ M^{-1} and the limit of detection was 7.1 μM. Moreover, Sn^{4+} sensing by probe **3** was reversible in nature as confirmed by Na_2S and EDTA titration experiments. The authors created test kits to detect Sn^{4+} ions with the naked eye. This probe was successfully employed in cell imaging studies. The authors also reported a control molecule (**4**) that showed a negligible response towards Sn^{4+} detection (only a 3.7-fold fluorescence enhancement).

In 2015, Cheng *et al.* developed two rhodamine derivative-based probes **5** and **6** that sensed Sn^{4+} ions in the EtOH/HEPES (1 mM, pH 7.4, 1 : 1, v/v) solvent system.[81] Probe **5** was selectively and sensitively bound to Sn^{4+} ions with a turn-on fluorescence change among other competitive metal cations. A 49.2-fold increase in the emission intensity at 582.2 nm displayed a linear response to 1–16 μM Sn^{4+}, with a limit of detection of 0.9 μM. Moreover, kinetic studies confirmed that the sensing process was completed within 1 min. This outcome was due to the coordination of Sn^{4+} ions at three O binding sites in the probe (1 : 1 stoichiometry) for the opening of the spirocyclic ring (Fig. 3). They used mass and FT-IR spectroscopy to validate the metal induced complexation and its mechanism. Similarly, the addition of Sn^{4+} into the organoaqueous solution of probe **6** induced comparable properties to probe **5**. However, the reversibility was also proved by adding sodium sulphide

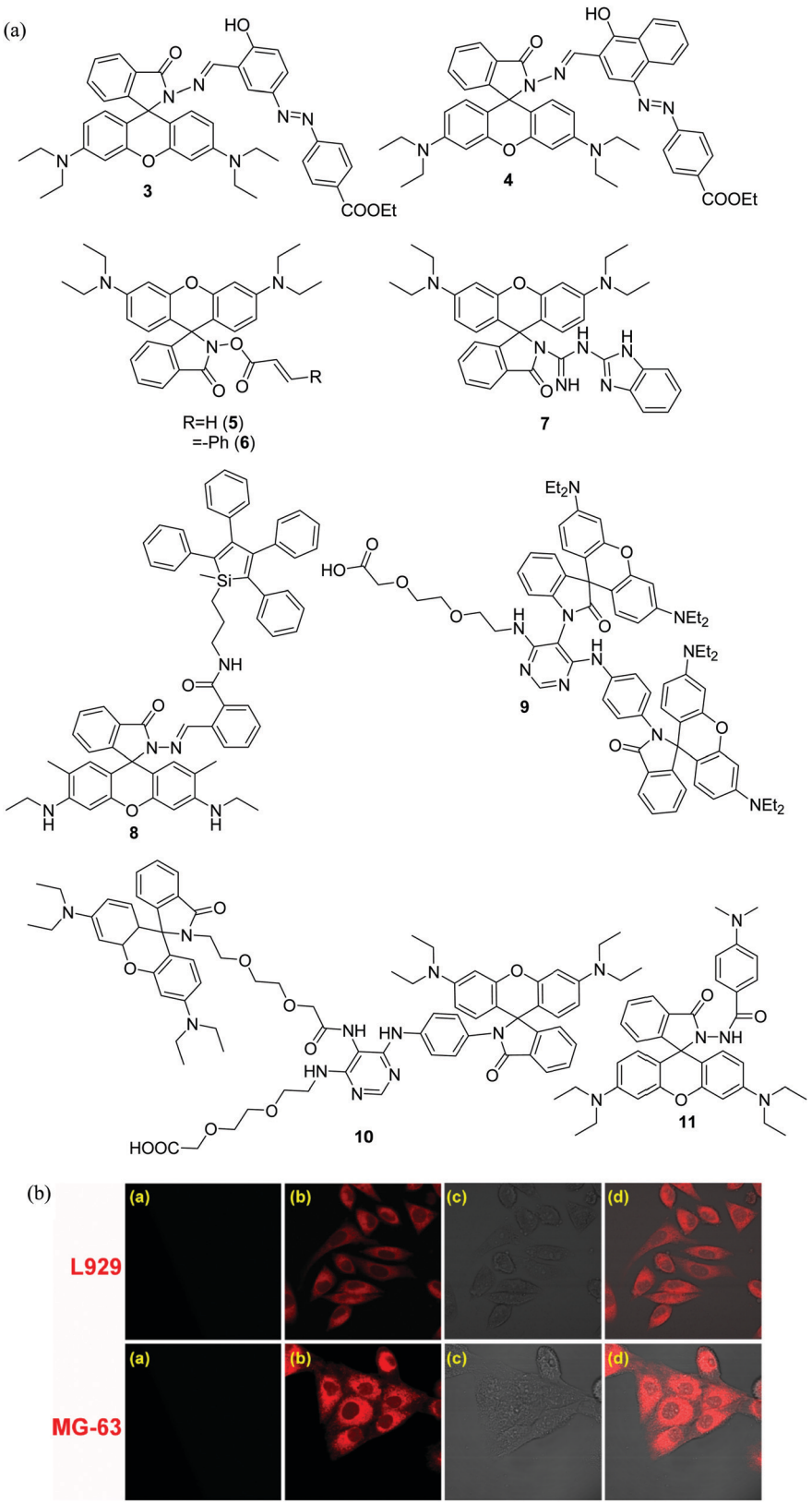

Fig. 3 (a) Chemical structures of probes **3–11**. (b) Fluorescence images of L929 mouse fibroblast cells and human osteosarcoma MG-63 cells (a: only probe, b: probe + $SnCl_4$, c: bright field image of probe **7** and $SnCl_4$, d: overlay images of b and c). Reprinted from ref. 82. Copyright (2017), with permission from Elsevier.

solution to the metal complex solution. Furthermore, probe **5** was employed to image Sn^{4+} in MGC-803 cells.

Yang *et al.* synthesized and reported a rhodamine derivative **7** that acts as a specific and sensitive reversible sensor for Sn^{4+} ions in an EtOH–H_2O (5/5, v/v, PBS, pH 7.4) mixed solution.[82] Among the different metal cations, probe **7** revealed a colorimetric change as well as fluorescence enhancement at 581 nm only for Sn^{4+} ions, while there were comparatively minor fluorescence responses with Pb^{2+}, Fe^{3+} and Cr^{3+}. From a time-dependent analysis, the authors verified that complex formation between the probe and Sn^{4+} was achieved within 10s. The binding stoichiometric ratio between **7** and Sn^{4+} was defined to be 1 : 1 using Job's plot analysis. The association constant of probe **7** towards Sn^{4+} was calculated as 2.99×10^6 M^{-1}. Furthermore, the relative absorbance along with emission intensities showed excellent linear relationships with the Sn^{4+} concentration (0.06–50 μmol L^{-1}) and the limit of detection was estimated to be 0.03 μmol L^{-1}. Due to its superior cell-membrane permeability and slight cytotoxicity, the probe was effectively used to image Sn^{4+} ions in L929 mouse fibroblast cells and human osteosarcoma MG-63 cells (Fig. 3).

In 2019, Wang *et al.* developed a DRET (dark resonance energy transfer) platform (**8**) for Sn^{4+} detection in MeOH/H_2O (9 : 1, v/v) solution.[83] In this system, silole acted as a DRET donor and the rhodamine moiety was the DRET acceptor. The probe showed a major and a minor absorption peak centred at 303 nm and 356 nm, respectively, indicating that the rhodamine unit exclusively persisted in its closed spirolactam form. However, upon addition of Sn^{4+} there was a significant increase in absorption intensity at 530 nm, resulting in a change in color from colorless to pink, indicating the formation of a ring opened amide structure. Now, upon excitation at 356 nm, a very weak emission of **8** was observed due to the non-fluorescence features of the spirocyclic structure of the rhodamine unit and the AIE nature of the silole unit. Furthermore, adding Sn^{4+} to an organo-aqueous solution of probe **8** led to significantly increased fluorescence at 554 nm through the DRET technique from the donor silol moiety to the ring-opened conjugated form of the rhodamine acceptor moiety. The suggested sensing mechanism was proved by ^1H NMR titration, FT-IR and mass spectral studies. The detection limit and stoichiometry of **8** to Sn^{4+} were 1.45 μM and 1 : 1, respectively. The ^1H NMR titration, FT-IR, and mass spectral studies all supported the proposed sensing mechanism. Probe **8** to Sn^{4+} had a detection limit of 1.45 M and a stoichiometry of 1 : 1. In addition, when Na_2S solution was added to this complex, it caused reversible variations in the fluorescence and absorption spectra (Fig. 3).

Two rhodamine-based probes **9** and **10** were reported by the Hlavac group as Sn^{4+} chemosensors.[84] Upon addition of Sn^{4+}, both probes exhibited a large fluorescence enhancement at 583 nm as a result of the Sn^{4+}-assisted spiro ring opening of the rhodamine moiety. Similarly, when Sn^{4+} was added to the organo-aqueous solution (MeOH/H_2O, 2 : 1, v/v) of probe **9**, the absorbance band at 560 nm increased gradually, accompanied by a color change from colorless to pink. The authors suggested the formation of 1 : 1 (probe : Sn^{4+}) and 3 : 2 (probe : Sn^{4+}) complexes for probes **9** and **10**, respectively. From fluorescence titration studies, the association constants for binding of Sn^{4+} ions by probes **9** and **10** were calculated to be 1.57×10^4 and 1.63×10^4 M^{-1}, respectively. Furthermore, probes **9** and **10** were found to have detection limits of 2.78 and 2.56 M, respectively (Fig. 3).

Ramakrishnappa and coworkers reported very recently a rhodamine-B based compound **11** as a colorimetric and a fluorometric probe for Zn^{2+} and Sn^{4+} ions, respectively.[85] When probe **11** was present in the closed ring form, it is indeed non-fluorescent; however, in the presence of Sn^{4+} ions, the spirolactam ring opens, causing a significant enhancement in the fluorescence spectra at 583 nm (λ_{ex} = 553 nm). The emission intensity at 583 nm linearly increased with the concentration of Sn^{4+} in the range of 1–100 nM, and the detection limit was determined as 0.174 nM. Moreover, 1 : 1 complexation between the probe and Sn^{4+} was confirmed by Job's plot and mass spectroscopy. Additionally, sensor **11** was employed in the development of molecular logic gates (Fig. 3).

2.1.2. Miscellaneous chemosensors. A pyrene thiazole conjugate **12** for Sn^{4+} detection was reported by Mahapatra and co-workers.[86] In UV-vis experiments, upon addition of Sn^{4+} ions to an EtOH–H_2O (4 : 1, v/v, HEPES buffer, pH 7.4) solution of probe **12** resulted in a decrease in the absorbance band at 242, 277 and 344 nm, accompanied by a color change from pale yellow to colorless. Probe **12** was weakly fluorescent owing to the PET process from the amine group N atom to the pyrene moiety (Fig. 4). However, the fluorescence of this probe turned highly deep sky-blue in the presence of Sn^{4+} as a result of the formation of a 2 : 1 complex (probe : metal) that eliminated the PET mechanism. The Job's plot experiment proved the 2 : 1 stoichiometry of the Sn^{4+} complex. The detection limit of **12** for Sn^{4+} was 6.93 μM. The proposed binding mechanism was determined by ^1H NMR titration, DFT and mass spectroscopy studies. In addition, binding of Sn^{4+} to probe **12** was reversible in nature. Addition of Na_2S or EDTA solution to the *in situ* prepared tin complex [**12**–Sn^{4+}] solution led to the restoration of the initial color and fluorescence of probe **12**. Moreover, confocal microscopy imaging experiments suggested that probe **12** was able to image Sn^{4+} ions in Vero 76 cells.

A fluorescent chemosensor **13** for reversible sensing of Sn^{4+} and PO_4^{3-} ions was developed by Liu *et al.*[87] Probe **13** was almost non-fluorescent (quantum yield = 0.005) but a 12-fold enhancement of fluorescence intensity at 489 nm (quantum yield = 0.062) was noticed in the presence of Sn^{4+} ions. This was due to the formation of a 1 : 1 complex between the probe N atom and Sn^{4+}, reinforcing the internal charge-transfer (ICT) process. According to Job's plot analysis, the stoichiometry between **13** and Sn^{4+} was indeed 1 : 1. The binding constant (K_s), calculated by using nonlinear least-squares analysis was 4.7×10^4 M. According to the fluorescence titration data, the detection limit was calculated to be 4.71×10^{-5} M. Moreover, to verify the interaction nature, ^1H NMR titration was performed. Probe **13** was found to have a high selectivity to Sn^{4+} over other metal cations (Na^+, K^+, Mg^{2+}, Ca^{2+}, Zn^{2+}, Cd^{2+}, Hg^{2+}, Co^{2+}, Ag^+, Ni^{2+}, Mn^{2+}, Fe^{2+}, Cu^{2+}, and Pb^{2+}) except that Cr^{3+} and Fe^{3+}

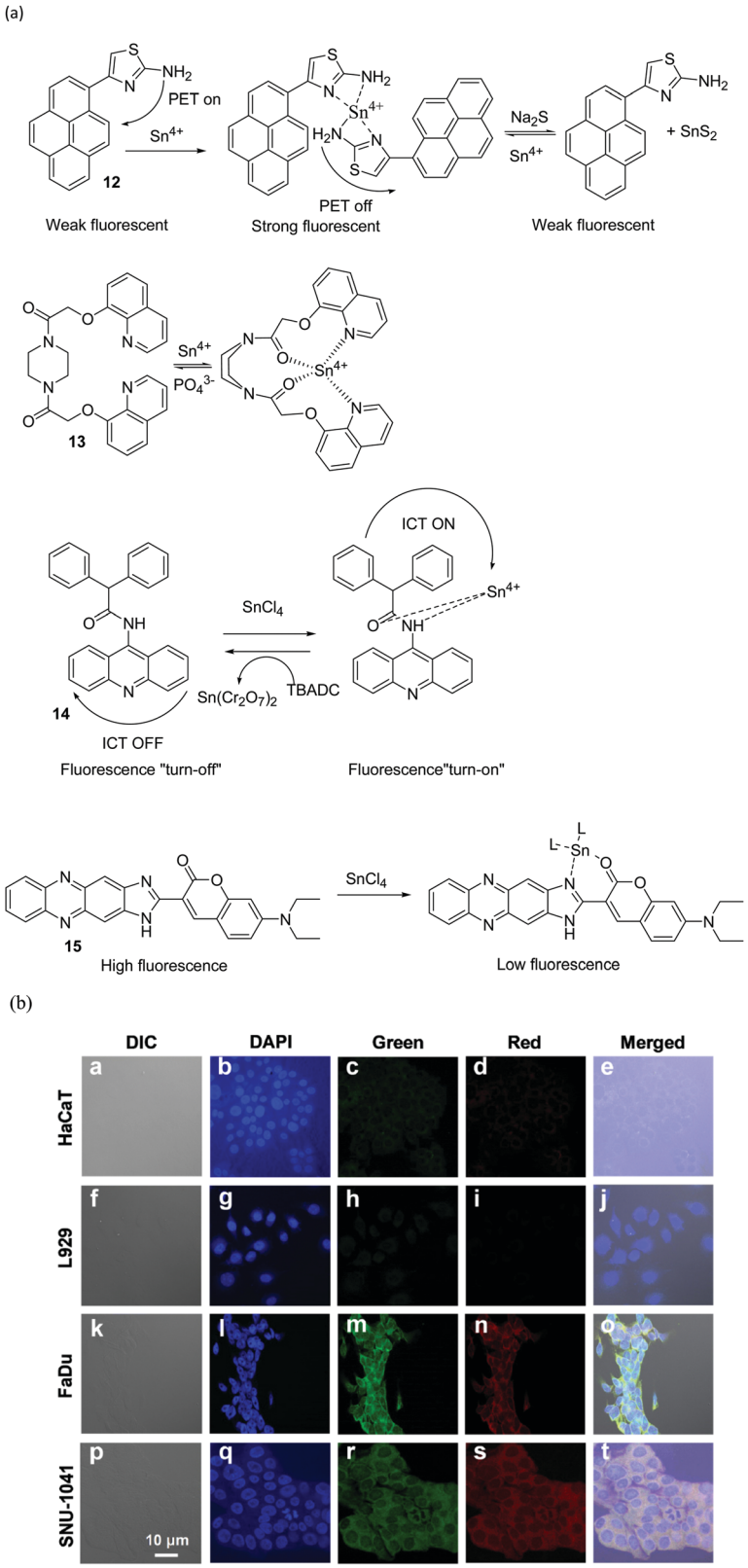

Fig. 4 (a) Chemical structures of probes **12–15** and their probable sensing mechanisms. (b) Confocal fluorescence microscopy images of HaCaT, L929, FaDu, and SNU-1041 cells in the presence of probe **14** and Sn^{4+}. Reprinted from ref. 88. Copyright (2021), with permission from Elsevier.

somewhat responded to chemosensor **13**. Moreover, the formation of the complex (**13**–Sn^{4+}) was found to be reversible in the presence of PO_4^{3-} (Fig. 4).

An acridine–diphenylacetyl based Sn^{4+}-selective chemosensor **14** was designed and reported by Ravichandiran *et al.*[88] In aqueous solution, probe **14** displayed a 2.96-fold fluorescence enhancement toward Sn^{4+} ions owing to the ICT (intramolecular charge transfer) mechanism and exciplex complex formation. The absorption spectra of **14** exhibited four peaks at 252, 265, 357, and 374 nm. Furthermore, upon addition of Sn^{4+}, a red-shifted absorption band (from 252 to 258 nm) was found. Besides, blue-shifted absorption signals were observed from 357nm to 342 nm and from 374 to 360 nm with an excellent linear relationship curve (R^2 = 0.9934). In the presence of other ionic species, the absorption and emission wavelengths of the probe remained unchanged. The suggested binding mechanism (1 : 1, **14** : Sn^{4+}) was well supported by Job's plot, ^{1}H NMR, FT-IR, and field emission scanning electron microscopy (FE-SEM) experiments and DFT calculations. The binding constant and detection limit were found to be 1.0 × 10^6 M^{-1} and 0.268 μM, respectively. According to the biological findings, probe **14** was cell permeable and capable of discriminative identification of Sn^{4+} ions in human normal and cancer cells. Additionally, this probe was utilized for the Sn^{4+} quantification in real water samples. In FaDu cells, **14** was also found to operate as a mitochondria-targeted probe. Moreover, **14**–Sn^{4+} was successfully utilized for detection of $Cr_2O_7^{2-}$ ions (Fig. 4).

Zhu *et al.* developed a coumarin derivative based probe **15** that can detect Sn^{4+} ions in a fluorescence turn-off manner.[89] Upon binding with Sn^{4+} ions, the emission spectrum of **15** at 585 nm was quenched along with a red shift in the absorption spectrum (from 475 nm to 523 nm) in a DMSO–water (9 : 1, v/v) solution. Sensor **15** was also employed to image Sn^{4+} ions in living HeLa cells (Fig. 4).

2.2. Sn^{2+} chemosensors

2.2.1. Rhodamine-based chemosensors. In this section, we have reported six rhodamine-based chemosensors for Sn^{2+} ions.

Adhikari's group developed a TBET based ratiometric fluorescent chemosensor **16** for Sn^{2+} utilizing the sensing mechanism of Sn^{2+}-induced spirocyclic ring opening of the rhodamine moiety.[90] Initially, the free probe apparently exhibited an absorption maximum at 323 nm in a 1 : 4 acetonitrile : HEPES buffer (10 mM, pH 7.4) solution. After the gradual addition of Sn^{2+}, the absorption band at 323 nm decreased, and concurrently the absorption band at 556 nm increased, resulting in visible color changes from colorless to pink. However, on addition of Sn^{2+} to the mixed solution of probe **16**, the initial emission band at 442 nm decreased and a new band appeared at 599 nm (red-shifted by 157 nm, λ_{ex} = 366 nm), resulting from the Sn^{2+} triggered spirolactam ring opening of the rhodamine unit as shown in Fig. 5. Meanwhile, after binding with Sn^{2+}, the fluorescence quantum yield of **16** increased from 0.02 to 0.330. Job's plot suggested that **16** interacts with Sn^{2+} ions *via* a 1 : 1 binding mode. The sensing process was also authenticated by ^{1}H NMR, mass spectroscopy and DFT calculations. The association constant was determined as

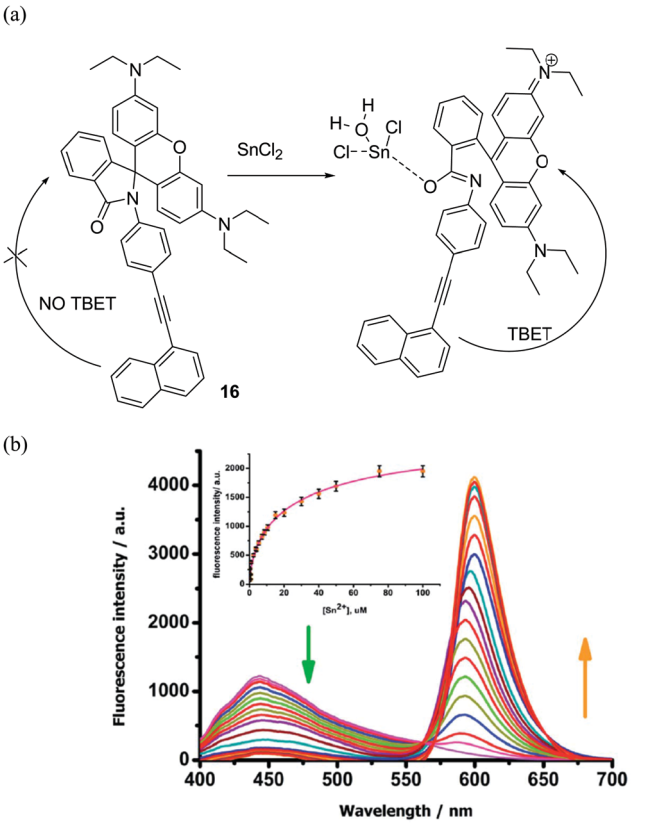

Fig. 5 (a) Chemical structure of probe **16** and its proposed sensing mechanism. (b) Emission intensity changes of probe **16** upon gradual addition of Sn^{2+} in acetonitrile–HEPES solution (1 : 4, v/v, 10 mM, pH = 7.4, λ_{ex} = 366 nm; inset: emission intensity *vs.* concentration graph). Reproduced from ref. 90 with permission of The Royal Society of Chemistry.

3.1 × 10^5 M^{-1} using the Benesi–Hildebrand equation. Besides this, probe **16** was shown to have a detection limit for Sn^{2+} as low as 5 × 10^{-9} M (5 nM). In the presence of other competing species (Hg^{2+}, Zn^{2+}, Pb^{2+}, Mn^{2+}, Ag^{+}, Au^{+}, Co^{2+}, Al^{3+}, Ni^{2+}, Ca^{2+}, Cu^{2+}, Cd^{2+}, Cr^{3+} and Fe^{3+}), **16** exhibited good selectivity. In addition, this cell permeable probe was utilized to sense Sn^{2+} ions in RAW 264.7 cells.

In 2014, Lan *et al.* developed two rhodamine-based chemosensors **17** and **18** (Fig. 6) for detection of toxic Sn^{2+} ions.[91] Both free probes were nonfluorescent due to their spirocyclic structure. The rhodamine emission peak at 580 nm was significantly increased with a concomitant emission colour change from colourless to orange when Sn^{2+} ions were added to a solution of probes **17** and **18**. The quantum yield was enhanced from 0.076 to 0.237 for **17** and from 0.066 to 0.187 for **18** after interaction with Sn^{2+}. With the addition of Sn^{2+}, the absorption band at 560 nm was enhanced, and the colour of the solution changed from colourless to pink, which was clearly visible to the naked eye. Both probes illustrated an excellent selectivity to Sn^{2+} over the other competing species, except that Cr^{3+} faintly responded to both probes. Mass spectroscopy and Job's plot suggested that both probes bind with Sn^{2+} ions in a 1 : 1 fashion. The association constants were calculated as 4.4 × 10^4 and 3.8 × 10^4 for **17** and **18**, respectively. The limits of

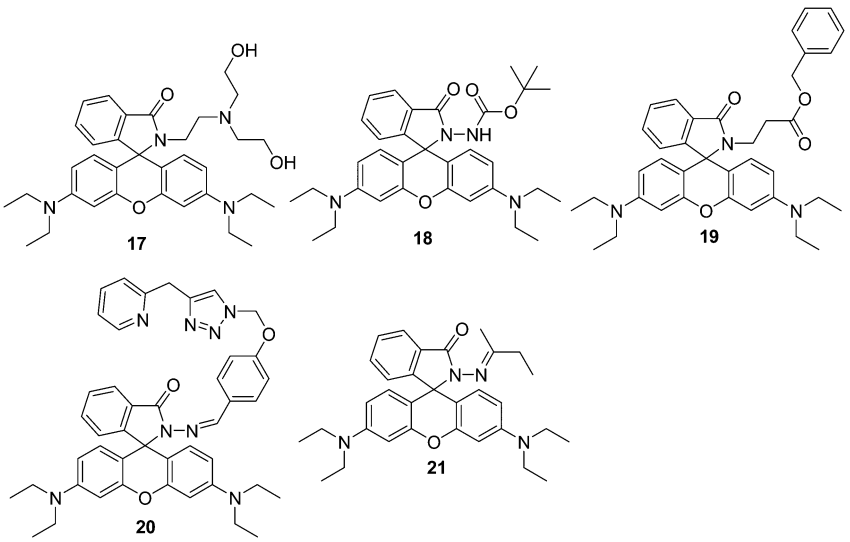

Fig. 6 Chemical structures of probes **17–21**.

detection of **17** and **18** were found to be 5.7×10^{-7} M and 4.6×10^{-7} M, respectively. Moreover, these two probes were successfully utilized for imaging Sn^{2+} in eukaryotic (live KB cells) and prokaryotic (live *Streptococcus mutans* cells) cells.

Bao's group developed and synthesised a rhodamine-based probe **19** that could efficiently and selectively detect Sn^{2+} ions *via* a spirolactam ring opening reaction of the rhodamine unit in a mixed ($MeOH/H_2O$, 2 : 3, v/v, pH 5.95) solution.[92] In the presence of Sn^{2+}, the absorption intensity of probe **19** increased significantly at 561 nm, and the colourless probe turned pink. After adding 5 equiv. of Sn^{2+} to the probe solution, the fluorescence intensity of the probe increased 300-fold at 583 nm. From the Job's plot experiment, the stoichiometry of **19** : Sn^{2+} was obtained, showing a 1 : 1 combination. The binding constant was measured as 2.65×10^4 M^{-1}. The limit of detection was reported as 0.044 μM (Fig. 6).

Yan *et al.* developed a rhodamine derivative **20** bearing the triazole-pyridine unit for the detection of Sn^{2+} in a mixed (CH_3CN/H_2O, 99/1, v/v) solvent.[93] In an organo-aqueous solution, the binding interaction between **20** and Sn^{2+} resulted in a progressive increase in absorption intensity at 560 nm, as well as a color change from colorless to pink. The fluorescence response of **20** to Sn^{2+} produced a red-shifted emission with a wavelength shift from 577 to 587 nm owing to the Sn^{2+}-induced ring opening of the spirolactam unit of probe **20** (Fig. 6). Moreover, this red shift in the emission spectrum caused the solution colour to change dramatically from colorless to orange, which could be recognised by the ''naked eye''. Job's plot and the HRMS study suggested a 1 : 1 stoichiometry between **20** and Sn^{2+}. ^1H NMR titration and DFT studies were performed to identify the probable sensing mechanism. The detection limits for Sn^{2+} were found from the fluorometric and colorimetric titration data to be 2.6×10^{-8} mol L^{-1} and 1.2×10^{-7} mol L^{-1}, respectively. The binding constant determined between **20** and Sn^{2+} was 1.2×10^6 M^{-1}, demonstrating a very significant binding affinity to Sn^{2+}. This probe displayed excellent selectivity to Sn^{2+} over Cr^{3+}, Hg^{2+}, Fe^{3+}, Co^{2+}, Ni^{2+}, Cu^{2+}, Bi^{3+}, Ba^{2+}, Al^{3+}, Mn^{2+}, Zn^{2+}, Pb^{2+}, Ca^{2+} and Cd^{2+}.

Tan and coworkers developed a rhodamine-based chemosensor **21** for Sn^{2+} and Al^{3+} detection (Fig. 6).[94] Upon incremental addition of Sn^{2+} and Al^{3+} to a solution of probe **21** in 30% acetonitrile solution, the absorption band increased gradually at 563 nm. This optical behaviour change was related to a change in colour from colorless to pink that could be seen by the naked eye. A noticeable enhancement in the emission spectra at 588 nm was also observed and was associated with a visually detectable color change from colorless to orange. Increases in fluorescence and absorbance spectra were associated with the metal-triggered spirolactam ring opening of the rhodamine unit. Job's plot and ESI-MS suggested 1 : 1 binding (**21** : Sn^{2+}) and the association constant was calculated as 2.72×10^6 M^{-1}. The detection limit of probe **21** for Sn^{2+} was estimated to be 5.10 μM. Furthermore, the sensing mechanism was also confirmed by FT-IR, ^1H NMR and ^{13}C NMR spectra. Additionally, this Sn^{2+} sensing mechanism was reversible in the presence of Na_2EDTA. The authors also constructed test strips for the sensing of metal cations (Sn^{2+} and Al^{3+}).

2.2.2. Naphthoquinone-based chemosensors. The naphthoquinone core is found in a wide range of natural organic compounds, including plumbagin, menadione, and lawsone.[95] Using naphthoquinone derivatives also has a lot of benefits. They have high molecular absorption coefficients, large fluorescence quantum yields, good fluorescence properties, and low toxicity to living cells. In this part, we reported 1,4-naphthoquinone-based 'turn-on' fluorescent/colorimetric chemosensors for Sn^{2+} ions.

Ravichandiran *et al.* developed a chromogenic and fluorogenic probe **22** for Sn^{2+} ions.[96] The Sn^{2+}-induced reduction of the –C═O– moiety to the –C–OH moiety, followed by 1 : 1 binding with Sn^{2+} ions, resulted in a remarkable 43-fold increase in the emission spectrum at 397 nm (Fig. 7). The fluorescence intensity of probe **22** demonstrated an excellent linear relationship with the Sn^{2+} concentration in the range of

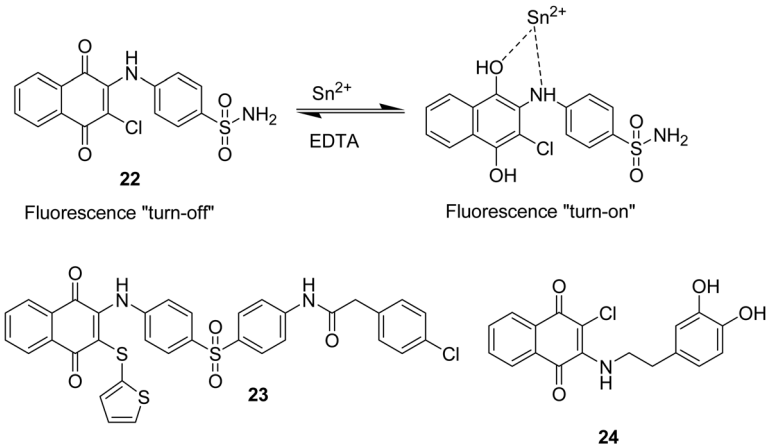

Fig. 7 Chemical structures of probes **22–24** and the probable binding interaction of probe **22** with Sn^{2+}.

0 to 62.5 μM and a limit of detection of 0.115 μM. The binding constant was 5.0×10^6 M^{-1} which was calculated using the Benesi and Hildebrand equation. This sensing mechanism was supported by ^{1}H NMR, ^{13}C NMR, mass, and FT-IR spectroscopy and cyclic voltammetry experiments. Confocal bioimaging experiments confirmed that probe **22** was applied to monitor trace amounts of Sn^{2+} ions in zebrafish and human living cells. This probe was sucessfully used for the discriminative detection of tin ions in human cancer cells from normal live cells.

Subsequently, in 2021, the same group developed an AIE- and ICT-based mitochondria targeted colorimetric and "turn-on" fluorescent probe **23** for Sn^{2+} detection.[97] On excitation at 280 nm, initially the probe emitted weak fluorescence in a buffered aqueous solution. However, probe **23** showed a notable fluorescence enhancement (36-fold) at 400 nm upon binding with Sn^{2+} *via* a 1 : 1 binding stoichiometry (Fig. 7). The Job's plot and mass spectroscopy analysis revealed a 1 : 1 complex stoichiometry. A LOD of 79 nM for Sn^{2+} with an association constant of 2.5×10^6 M^{-1} was determined. The sensing mechanism is based on the reduction of the ketone (–C═O) to hydroxyl (–C–OH) group at the naphthoquinone moiety by Sn^{2+}, resulting in a dramatic color change from light maroon to milky white. The sensing pathway was very fast and approximately complete within 10 s. Moreover, this fluorescence change was found to be reversible in the presence of EDTA. ^{1} H NMR, FT-IR, and theoretical results were used to confirm the sensing mechanism. Furthermore, the cell imaging experiments suggested that this probe could be used to detect Sn^{2+} selectively in human cells and zebrafish larvae. Most interestingly, the probe was utilized for the discriminative recognition of tin ions in human cancer cells and normal living cells.

In 2020, a naphthoquinone–dopamine hybrid (**24**) was utilized as a Sn^{2+} chemosensor by Yoo's group.[98] Due to the retardation of the PET effect, adding Sn^{2+} to an aqueous solution of probe **24** (20 mM HEPES, pH = 7.5) resulted in a 49-fold increase in fluorescence (Fig. 7). A number of potentially competing analytes did not appear to interfere with this probe, except that Fe^{2+} and Fe^{3+} modestly responded to probe **24**. A 1 : 1 stoichiometry between **24** and Sn^{2+} was determined through Job's plot analysis. Furthermore, an association constant of 1.42×10^6 M^{-1} was determined for binding between probe **24** and Sn^{2+} ions using the Benesi–Hildebrand equation. The detection limit was calculated as 4.13×10^{-7} M, and the response time was less than 5s. Sn^{2+} was also imaged in live HaCaT cells and zebrafish using probe **24**. Additionally, this probe was capable of distinguishing between normal and cancerous human cells.

2.2.3. Diarylethene-based chemosensors. Generally, the structure and properties of photochromic compounds can be altered when they are irradiated with light of different wavelengths. Among numerous photochromic compounds, diarylethene derivatives garner the most interest from researchers because of their high fatigue resistance, superior thermal stability, quick response time, excellent quantum yield and lack of thermal isomerization.[99] Due to these features, diarylethene-based compounds have a wide range of applications (such as optoelectronic devices, chemosensors, and so on) in a variety of fields. Various diarylethene-based fluorescent chemosensors have recently been reported.[100] Chemosensors based on diarylethene derivatives for Sn^{2+} ions are presented in this section.

Very recently, Liu *et al.* reported two diarylethene–styrene-linked pyrido[2,3-*b*] pyrazine conjugates **25** and **26** for the recognition of Hg^{2+} and Sn^{2+} in the CH_3CN solvent.[101] In the presence of Sn^{2+} only, probe **25** did not show any colorimetric or absorption spectral changes. However, upon addition of Sn^{2+} (17.25 equiv. for **25**) to the solution of **25**–Hg^{2+}, the absorbance was meaningfully blue-shifted with a simultaneous color change from yellow to colourless owing to the formation of the **25**–Sn^{2+} complex (Fig. 8). A similar observation was obtained when 25.75 equiv. of Sn^{2+} was added to the solution of **26**–Hg^{2+}. The detection limits of **25**–Hg^{2+} and **26**–Hg^{2+} for Sn^{2+} were calculated using the absorption data to be 1.54×10^{-7} M and 3.64×10^{-8} M, respectively. The fluorescence intensity of the **25**–Hg^{2+} solution increased significantly (quantum yield = 0.186) after the addition of Sn^{2+} ions and the color of the mixture changed from dark green to bright yellow. The limit of detection for Sn^{2+} was found to be as low as 5.44×10^{-6} M. The authors used ^{1}H NMR titration studies to prove the sensing mechanism.

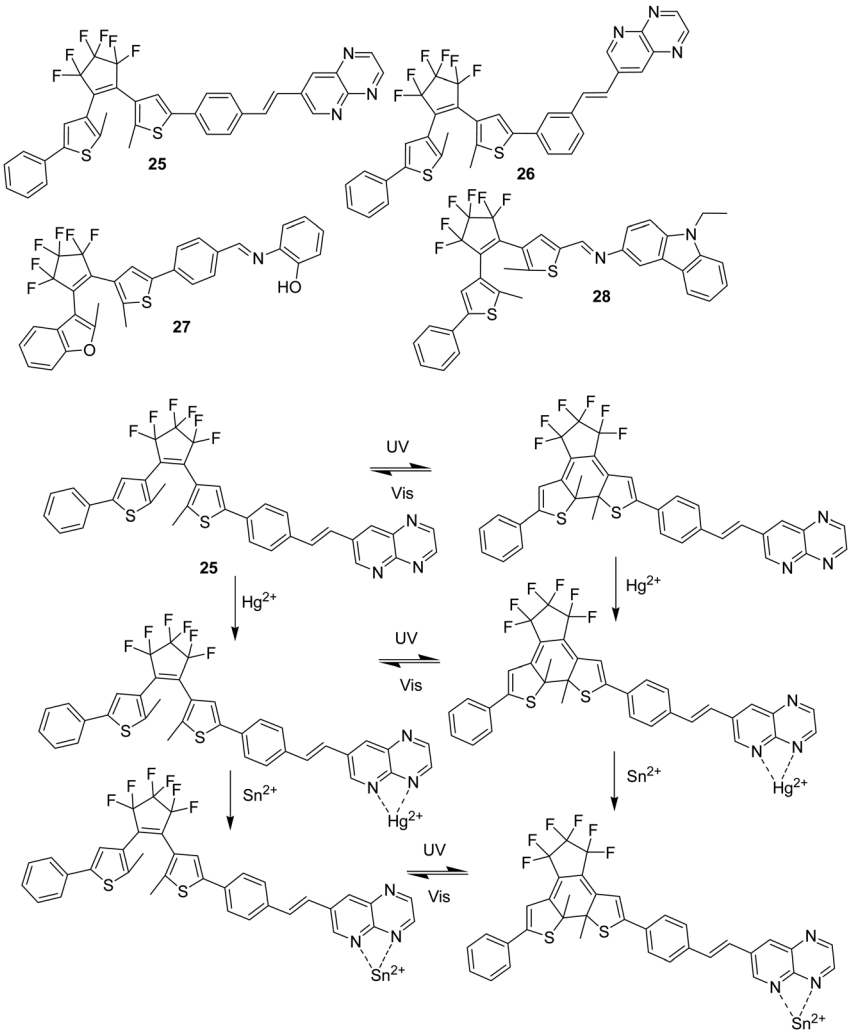

Fig. 8 Chemical structures of probes **25–28** and the probable sensing mechanism of probe **25** with Sn^{2+}.

Chemosensor **27**, reported by Pu *et al.*, was responsive to toxic Sn^{2+} ions.[102] In the presence of Sn^{2+} ions, the fluorescence was gradually increased 8-fold at 454 nm in the methanol solvent *via* 1 : 2 (metal : probe) complexation. Moreover, other metal cations such as K^{+}, Ca^{2+}, Zn^{2+}, Pb^{2+}, Ba^{2+}, Mg^{2+}, Mn^{2+}, Ni^{2+}, Co^{2+}, Hg^{2+}, Al^{3+}, Cu^{2+}, Fe^{3+}, Cd^{2+}, and Cr^{3+} did not reveal any cation induced fluorescence enhancement under identical conditions. Besides, the fluorescence intensity of the **27**–Sn^{2+} complex was reduced markedly when irradiated with 297 nm light, attributed to the generation of the closed-ring moiety of **27**–Sn^{2+} (Fig. 8).

In 2017, Qu *et al.* reported a fluorescent chemosensor (**28**) for detecting Sn^{2+} (''turn-on'') and Cu^{2+} (turn-off) in methanolic solution.[103] In the presence of Sn^{2+} cations, a 76 nm blue shift was noticed in the emission wavelength of this probe owing to the emergence of the **28**–Sn^{2+} complex, accompanied by the inhibition of C=N isomerization. The generation of a 1 : 1 **28**–Sn^{2+} complex was predicted by Job's plot analysis and also verified by single ^{1}H NMR and mass spectral analyses. The probe detected Sn^{2+} in solution with a detection limit of 1.9 μM. Furthermore, this sensing process was reversible in nature. The authors also established that this probe could be used to determine Sn^{2+} ions in several water samples (Fig. 8).

2.2.4. Triphenylamine-based chemosensors. Triphenylamine (TPA) is a non-planar, propeller-shaped tertiary amine made up of three aromatic phenyl groups.[104] Although triphenylamine does not display a large amount of fluorescence emission, modified TPA derivatives have been used to make fluorescent probes and electroactive and optoelectronic materials because of their chemical stability, photoluminescence properties, thermal resistance, electroactive properties, and so on. Two triphenylamine-based probes for Sn^{2+} detection are described in this section.

Kaya and coworkers synthesized and reported a fluorescent triphenylamine derivative chemosensor **29** for highly selective Sn^{2+} detection in a DMSO/deionized H_2O (1 : 1, v/v) solution.[105] On excitation at 320 nm, the emission intensity of the non-fluorescent probe **29** increased notably (33-fold enhancement) at 460 nm in the presence of Sn^{2+} ions and the color of the mixture changed from yellow to deep blue. In the presence of Sn^{2+}, the fluorescence quantum yield of **29** was determined to be 24%. In the range of 1 mM to 3.9 μM, probe **29** showed a linear relationship between the emission intensity and Sn^{2+}

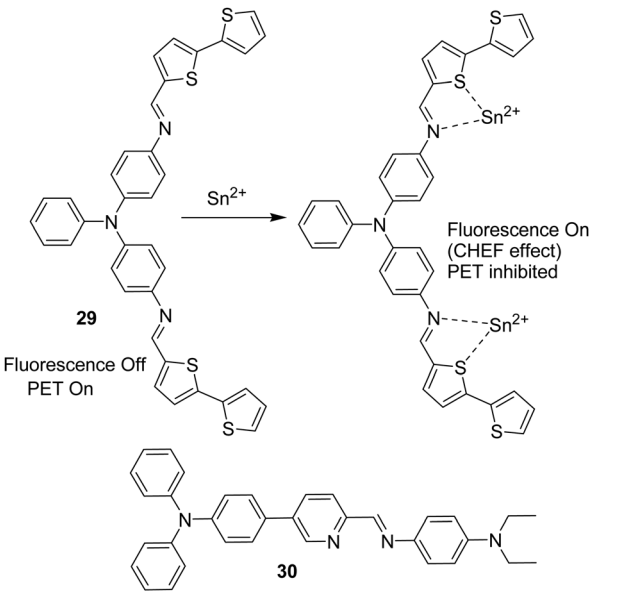

Fig. 9 Chemical structures of probes **29** and **30** and the probable binding interaction of probe **29** with Sn^{2+}.

concentration. The LOD of **29** for Sn^{2+} was reported as 3.14×10^{-7} M. The association constant was calculated as 6.8×10^{9} M^{-2} from the fluorescence titration data. This enhancement of the fluorescence intensity was mainly due to the cumulative result of suppression of the PET process owing to the Sn^{2+} triggered CHEF mechanism. The Job's plot analysis revealed 1 : 2 (**29** : Sn^{2+}) probe–Sn^{2+} complex formation (Fig. 9) which was further validated by mass spectral analysis. Moreover, in the presence of other competitive analytes, probe **29** did not show any spectral changes, indicating high selectivity of **29** toward Sn^{2+} ions.

Meng *et al.* developed an ICT-based colorimetric and fluorometric probe **30** for Sn^{2+} detection in THF solution.[106] The probe was obtained from the Schiff base condensation reaction between 5-(4-(diphenylamino)phenyl)picolinaldehyde and *N*,*N*-diethylbenzene-1,4-diamine in the ethanol solvent. Probe **30**, in the presence of Sn^{2+} (λ_{ext}= 420 nm), displayed a 63-fold enhancement in the fluorescence spectra at 561 nm. The quantum yield of **30** increased from 1.43% to 68.21% upon addition of Sn^{2+} ions. A good linear relationship was found between the fluorescence intensity at 561 nm and the concentration of Sn^{2+} in the range of 1 to 6 μM and the detection limit was found to be 0.116 μM. Job's plot exhibited a 1 : 1 stoichiometry of the **30**–Sn^{2+} complex and the corresponding association constant was calculated to be 1.6×10^{4} M^{-1}. Moreover, this detection mechanism was also supported by density functional theory (DFT) calculations and ^{1}H NMR titration. Other common competing metal cations did not interfere, except for Al^{3+}, Cr^{3+} and Fe^{3+}, which slightly increased the emission intensity. Furthermore, the probe was employed to monitor the intracellular Sn^{2+} in HeLa cells (Fig. 9).

2.2.5. Terpyridine-based chemosensors. Terpyridine (2,2′:6′,2″-terpyridine) is a well-known *N*-heterocyclic terdentate ligand for metal cations.[107] Terpyridine derivatives can be used as a versatile platform in the area of supramolecular and coordination chemistry because of their ease of synthesis and outstanding ability to bind with metal ions *via* appropriately arranged ring nitrogen atoms. Many chemosensors based on terpyridine derivatives for metal cations have been reported so far. Two terpyridine-based Sn^{2+} chemosensors are outlined in this section.

Very recently, Manivannan *et al.* developed a diketopyrrolopyrrole based probe **31** for the recognition of harmful Sn^{2+}, Co^{2+} and CN^{-} ions in a 1 : 1 v/v DMF/H_2O solution.[108] The free probe **31** presented three absorption bands at 283, 322 and 493 nm. With the addition of Sn^{2+}, the absorption band at 283 nm increased, the peak intensity at 322 nm disappeared, and a new peak at 349 nm appeared with a shift of the initial peak at 493–501 nm, resulting in a colour change from fluorescent orange to red. Probe **31** initially showed one emission band at 383 nm and a strong band at 571 nm after being excited at 322 nm. However, upon addition of Sn^{2+} ions, the emission peaks at 383 nm and 571 progressively decreased and disappeared completely after addition of 2 equivalents of Sn^{2+} ions. Probe **31** binds to Sn^{2+} ions in a 1 : 2 (**31** : Sn^{2+}) binding fashion (Fig. 10) according to Job's plot and mass spectroscopy data. The binding constant of **31** for Sn^{2+} was 4.43×10^{8} M^{-1}. The detection limit was found to be as low as 2.21×10^{-9} M. In addition, the authors designed an electronic eye (RGB – Arduino gadget) that can detect these toxic analytes effectively. Furthermore, probe **31** was utilized for the determination of toxic analytes in real water samples.

A terpyridine derivative-based colorimetric and fluorometric chemosensor **32** was developed by Son's group for the detection of Fe^{3+}, Co^{2+}, Hg^{2+} and Sn^{2+} ions in 80% aq. DMF solution.[109] In the presence of Sn^{2+}, the fluorescence intensity of the non-fluorescent **32** increased considerably, accompanied by a dramatic emission color change from colorless to white which could be seen with the naked eye. According to the Job's plot analysis, the binding stoichiometry between **32** and Sn^{2+} was found to be 1 : 1. The binding constant for this complex was very high (4.2×10^{5} M^{-1}), indicating a significant binding interaction between **32** and the Sn^{2+} ions. The limit of detection of **32** for Sn^{2+} was determined as 1.57×10^{-9} M. The binding stoichiometry was also confirmed by MALDI-TOF mass spectrometry analysis. Moreover, a **32**-based hydrogel and RGB sensor device was reported by the authors for the selective sensing of metal cations (Fe^{3+}, Co^{2+}, Hg^{2+} and Sn^{2+}). This sensor was also used to detect Fe^{3+}, Co^{2+}, Hg^{2+} and Sn^{2+} in real water samples (Fig. 10).

2.2.6. Miscellaneous chemosensors. In 2022, Sahoo and co-workers designed and synthesized an anthracene-based chemosensor for sensing of Sn^{2+} ions in a H_2O : CH_3CN (1 : 1, v/v, pH 7.2, 10 mM Tris–Cl buffer) solution.[110] When Sn^{2+} was added to the probe solution, the absorbance intensities at 312 nm and 404 nm decreased considerably. Furthermore, upon addition of Sn^{2+}, the increase in the emission intensity (31-fold) was noted due to the Sn^{2+} induced inhibition of the PET process and the activation of the CHEF effect. The limit of detection of **33** for Sn^{2+} was 90 nM. The Job's plot analysis suggested that **33** binds to Sn^{2+} in a 1 : 1 stoichiometry fashion

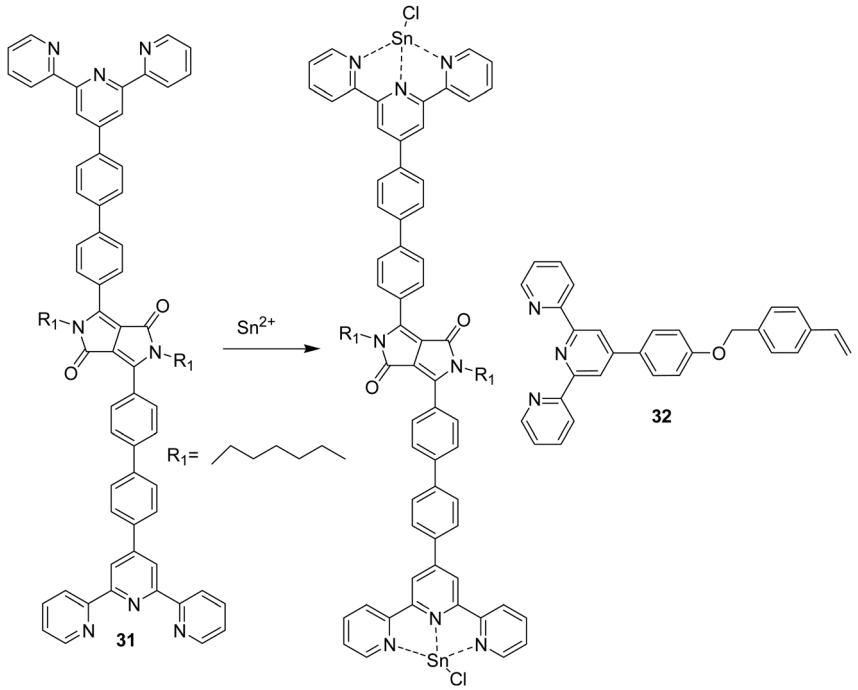

Fig. 10 Chemical structures of probes **31** and **32** and the probable binding interaction of probe **31** with Sn^{2+}.

and the binding constant was 1.60×10^6 M^{-1} (Fig. 11). Moreover, the sensing process was reversible as confirmed by EDTA experiments. This probe was also applied to determine the Sn^{2+} level in algal samples.

The same research group very recently reported a carbazole-naphthaldehyde based probe (**34**) for colorimetric recognition of Sn^{2+} ions in $CH_3CN:H_2O$ (1:8, v/v) at pH 7.0 (10 mM phosphate buffer) solution.[111] In the presence of Sn^{2+}, the initial absorption band at 400 nm decreased and a new absorption peak emerged at 454 nm with an isosbestic point at 425 nm. Probe **34** was able to detect Sn^{2+} with a concomitant color change from pale yellow to deep orange. These changes were mainly due to the non-covalent interactions between **34** and Sn^{2+}. The limit of detection for Sn^{2+} was deduced to be 85 nM. Probe **34** was able to detect Sn^{2+} preferentially over other cations. During complexation, a 1:1 adduct was established between **34** and Sn^{2+} according to the Job's plot data study. Moreover, the binding constant of **34** was estimated to be 0.35×10^6 M^{-1}, suggesting the strongest binding interaction with the Sn^{2+} ions. The authors also stated that **34** was used to sense and measure trace levels of Sn^{2+} in several mouthwash and toothpaste samples (Fig. 11).

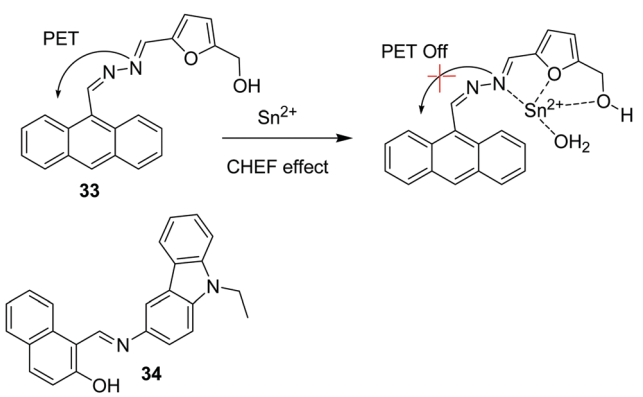

Fig. 11 Chemical structures of probes **33** and **34** and the probable binding interaction of probe **33** with Sn^{2+}.

A naphthalene derivative **35** responded to Sn^{2+} ions selectively (Fig. 12).[112] Probe **35** displayed weak monomer emissions at 420 nm with excitation at 330 nm in acetonitrile solution. On gradual addition of Sn^{2+} (up to 50 μM), the fluorescence intensity at 420 nm (monomer emission) increased, while a new band at 582 nm appeared which was ascribed to the intramolecular excimer formation between the two naphthalene moieties of **35**. Remarkably, increasing the concentration of Sn^{2+} (>50 μM) gradually decreased the monomer emission intensity at 420 nm while increasing the excimer emission at 582 nm (742-fold). In probe **35**, the intensity of the band at 380 nm decreased as more Sn^{2+} (>50μM) was added to the acetonitrile solution of **35**, whereas the absorption band at 501 nm increased significantly including an isosbestic point at 425 nm. The stoichiometric ratio of Sn^{2+} to **35** was measured to be 1:1 by Job's method and the association constant was found as $\sim 3.4 \times 10^5$. The detection limit for Sn^{2+} was found as 25.7 nM. Furthermore, probe **35** could even detect Al^{3+} in aqueous methanol by producing intense green fluorescence.

Velmathi *et al.* reported a salicylaldimine based chemosensor **36** for Sn^{2+}, Ni^{2+}, Fe^{3+}, Cu^{2+}, Co^{2+} and F^- ions in CH_3CN solution.[113] Upon gradual addition of Sn^{2+}, the absorbance band at 350 nm decreased, whereas a new absorption band at 420 nm appeared, including an isosbestic point at 360 nm. These

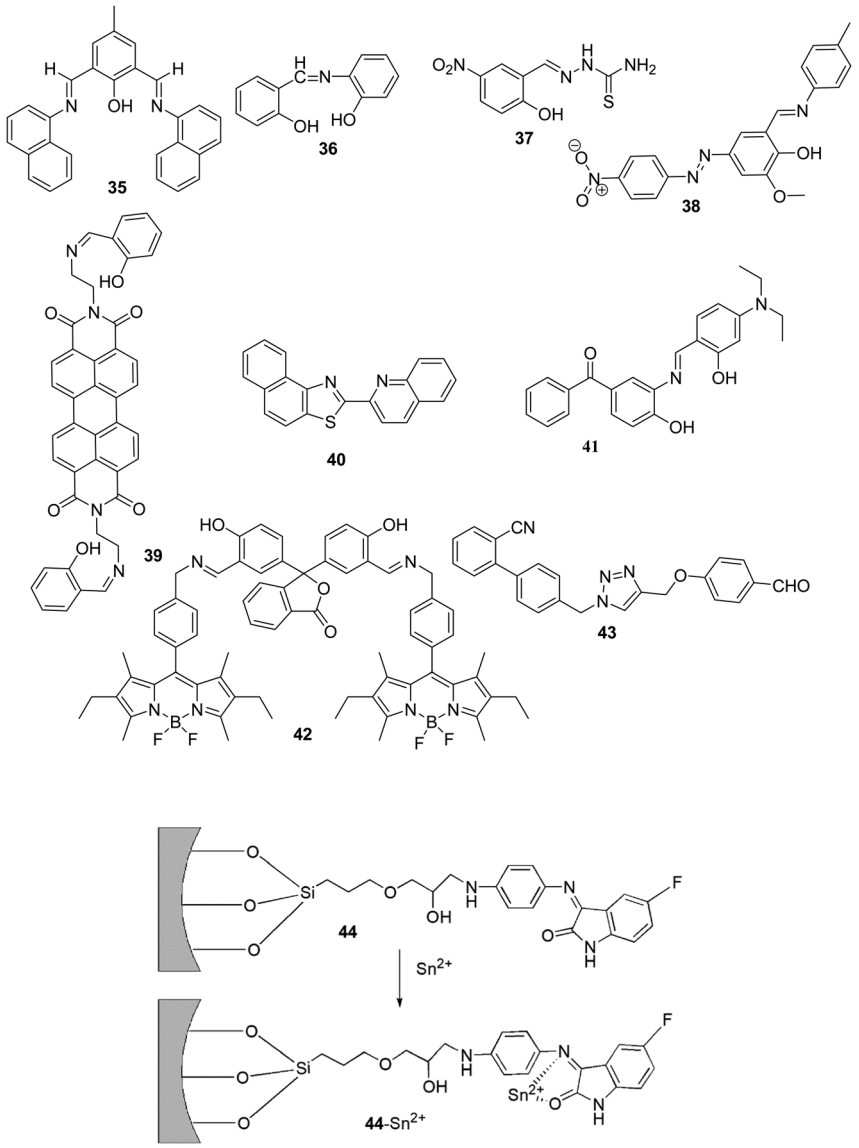

Fig. 12 Chemical structures of probes **35–44** and the probable binding interaction of probe **44** with Sn^{2+}.

absorption band changes were mainly due to the ligand to metal charge transfer (LMCT) complex formation. Meanwhile, the colorless probe displayed intense green fluorescence in the presence of 2 equiv. of Sn^{2+} ions. Moreover, 2 equiv. of Sn^{2+} caused a notable fluorescence enhancement at 500 nm. A 1 : 1 complex between the probe and Sn^{2+} formed (Fig. 12) according to the results of Job's plot experiments. The association constant was calculated as 3.008×10^3 M. The authors also reported another probe for sensing of Cu^{2+}, F^- and OH^- ions.

The same group used a similar strategy, [114] wherein a thiosemicarbazide-based probe **37** was used for Hg^{2+} and Sn^{2+} recognition in aqueous media (Fig. 12). Upon the gradual addition of Sn^{2+}/Hg^{2+} to the probe solution, the absorbance band at 210 nm was strengthened, whereas the bands at 310 nm and 450 nm were diminished. Probe **37** showed a very distinct color change from green to colorless due to the complexation between the probe and metal cations. In the presence of Hg^{2+}/Sn^{2+}, the emission band at 415 nm was enhanced which was attributed to the suppression of the PET process on metal complexation. The binding stoichiometry between **37** and Sn^{2+} was 1 : 1 according to Job's plot. The binding constant of **37** for Sn^{2+} was calculated as 1.48×10^4.

Ajalkar and coworkers reported a colorimetric dual sensor **38** for the recognition of CN^- and Sn^{2+} in an MeCN : bis–tris buffer (9 : 1, v/v; pH = 7.0) solution.[115] The absorbance at 283 nm was enhanced in the presence of Sn^{2+}, with an isosbestic point at 318 nm and the visible colour of the solution changing from yellow to colourless. By binding with phenolic oxygen and imine nitrogen atoms, probe **38** created a 2 : 1 complex with an Sn^{2+} ion (Fig. 12) and this binding pattern was confirmed by Job's plot, DFT calculations, and ^{1}H NMR, ESI-MS, and FT-IR spectroscopy analyses. The binding constant for Sn^{2+} was determined to be $K_a = 4.195 \times 10^3$ M^{-1}. The detection limit was observed to be 0.754 μmol L^{-1}, which is less

than that reported in the WHO guidelines for drinking water. The authors also made a test kit for solid state detection of Sn^{2+} ions.

In 2021, Ye *et al.* developed a perylene-based fluorescent probe **39** for Sn^{2+}.[116] Upon addition of Sn^{2+} to the DMF solution of probe **39**, the fluorescence intensity at 548 nm enhanced (38.4-fold) (Fig. 12). The binding process was confirmed by ^1H NMR titration and IR spectral data. The emission intensity had a wide linear range (50–100 μM) with the Sn^{2+} concentration with a LOD of 0.168 μM. Furthermore, in the presence of EDTA, the sensing probe was reversible.

A naphthothiazole-based probe **40** was designed for the sensing of Sn^{2+} and Zn^{2+} ions in solution and in living cells.[117] Probe **40** displayed a fluorescence intensity at 428 nm in CH_3CN–H_2O (80/20, v/v) solution. When Sn^{2+} ions were added, the emission peak red-shifted to 533 nm, associated with a colour change from blue to yellow. The fluorescence intensity at 533 nm was shown to have a strong linear relationship with the concentration of Sn^{2+} in the range of 0–5 μM and the detection limit was found to be as low as 8.21×10^{-8} M. As indicated by the Job's plot study, the stoichiometry of the complex formed between **40** and Sn^{2+} was determined to be 1 : 1, and the binding constant was measured as 7.5×10^5 M^{-1}. The probe's fluorescence response to Sn^{2+} allowed the imaging of Sn^{2+} in live *Scenedesmus obliquus* cells (Fig. 12).

In 2017, Jadhav *et al.* developed a benzophenone-based compound **41** as a fluorescent chemosensor for detection of Sn^{2+} in a THF–HEPES buffer (90 : 10, v/v, pH 7.4) solution.[118] When excited at 445 nm, Sn^{2+} induced an 18-fold increase in emission intensity (λ_{em} = 488 nm) owing to the CHEF effect and the suppression of PET, ESIPT and the C=N isomerisation process. In the presence of Sn^{2+}, the quantum yield increased from 0.62% to 79%. The Job's plot results indicated that the probe formed a 1 : 1 complex with Sn^{2+} which was further verified by a ^1H NMR titration study and theoretical calculations. The detection limit for Sn^{2+} and association constant of this complex was calculated as 0.3898 ppb and 1.50×10^4 M^{-1}, respectively. Other competitive metal cations (Ba^{2+}, Cu^{2+}, Pb^{2+}, Hg^{2+}, Mn^{2+}, Ni^{2+}, Fe^{3+}, Na^+, Al^{3+}, Ca^{2+} and Mg^{2+}) examined did not lead to a fluorescence response (Fig. 12).

A phenolphthalein based compound (**42**) appended with two BODIPY units was employed to sense Sn^{2+} and Al^{3+} ions in an acetone/H_2O (1 : 1) solution.[119] When excited at 370 nm, it exhibited weak fluorescence at 560 nm. Upon addition of Sn^{2+}/Al^{3+} ions, the fluorescence intensity was enhanced significantly at 560 nm. Probe **42** formed a 1 : 2 complex (probe : metal) as the metal cations (Sn^{2+}/Al^{3+}) were chelated with imine nitrogen and hydroxy groups of the phenolphthalein. Moreover, the sensing mechanism was also proved by ^1H NMR titration. The detection limits of **42** for Sn^{2+} and Al^{3+} were determined to be 6.31×10^{-8} M and 6.48×10^{-8} M, respectively. The Sn^{2+}/Al^{3+} recognition by probe **42** was reversible as confirmed by the EDTA titration experiment. Probe **42** was employed to detect Sn^{2+}/Al^{3+} ions using real water samples. Furthermore, the probe was utilized to sense Sn^{2+}/Al^{3+} in A549 cells (Fig. 12).

Singh *et al.* developed a triazole-containing probe **43** which showed a fluorometric response to Sn^{2+} ions in methanol solution.[120] Initially, probe **43** displayed two absorption bands at 208 nm and 260 nm. The band at 208 nm displayed a hyperchromic shift after consecutive addition of Sn^{2+} metal ions, whereas the band at 260 nm initially showed a hyperchromic shift, then a hypochromic shift, which was attributed to the electron density transfer between **43** and Sn^{2+}. Furthermore, the addition of Sn^{2+} resulted in an increase in fluorescence at 347 nm. Other competing cations did not produce UV-vis and fluorescence responses. The Job's plot analysis revealed a 1 : 1 **43**-to-Sn^{2+} stoichiometry. In addition, ^1H NMR and IR studies proved the selective binding of probe **43** with Sn^{2+} ions. The association constant and Stern–Volmer constant were determined as 13.36×10^5 M^{-1} and 12.6×10^6 M^{-1}, respectively. Using absorption and emission spectroscopy, the limit of detection was evaluated to be 0.47×10^{-7} M and 3.8×10^{-9} M, respectively (Fig. 12).

Cheng's group reported a Schiff base functionalized mesoporous silica with epoxypropoxyl units (**44**) for detecting Sn^{2+} in aqueous media.[121] In the presence of Sn^{2+}, this probe showed a remarkable fluorescence enhancement at 339 nm. In the meantime, the quantum yield of **44** also increased to 0.12 from 0.063 when it complexed with Sn^{2+} ions. The probe was also shown to be selective to Sn^{2+} over other metal cations, except Hg^{2+}, Cr^{3+}, Ni^{2+}, and Ba^{2+} which showed very slight responses. The fluorescence intensity at 339 nm demonstrated a linear relationship with Sn^{2+} concentrations from 0 to 80 μM and the detection limit was measured as 0.5 μM (0.06 ppm). The association

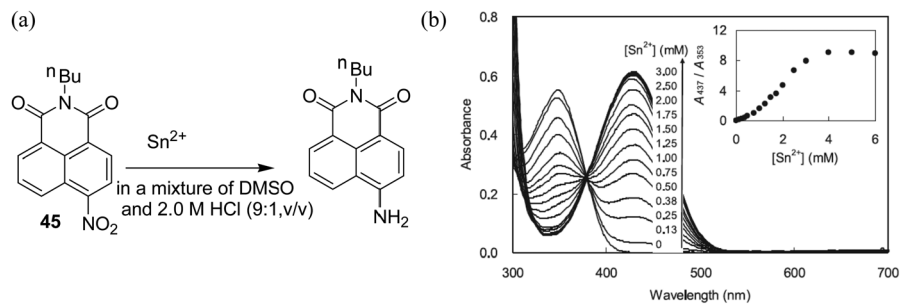

Fig. 13 (a) Chemical structure of probe **45**. (b) Changes in the absorption spectra of probe **45** in a DMSO and 2.0 M HCl (9 : 1, v/v) solution upon gradual addition of Sn^{2+}. Inset: Plot of the absorbance ratio change (A_{437}/A_{353}) *vs.* concentration. Reprinted from ref. 123. Copyright (2019), with permission from Elsevier.

Table 1 Summary of the sensing characteristics of tin ion (Sn^{4+}/Sn^{2+}) chemosensors (**1–45**)

Probe	Solvent	Sensing mechanism	Excitation (nm)	Emission in the presence of the analyte (nm)	Stoichiometry and association constant	Interference	Detection limit	Applications	Ref.
Sn^{4+} chemosensors									
1	Ethanol–HEPES (2 : 1, v/v)	Turn-on, FRET	420	523 to 580	1 : 1 and (4.73 ± 0.05) × 10^3 M^{-1}	Cu^{2+}, Cr^{3+}	1.1 × 10^{-5} M	Detection in living HeLa cells	78
2	CH_3OH/H_2O = 4 : 1, v/v, 10 μM HEPES buffer, pH = 7.4)	Turn-on	555	580	1 : 1 and 4.31 × 10^4 M^{-1}	—	2.58 μM	Detection in living RAW 264.7 cells	79
3, **4**	Aqueous ethanolic solution (HEPES, 10 mM, pH = 7.4, 1 : 4, v/v)	Turn—on	563 (**3**)	582 (**3**)	1 : 1 and 1.414 ± 0.41) × 104 M^{-1} (**3**)	—	7.1 μM (**3**)	(a) Detection in living RAW 264.7 cells, (b) test kits, and (c) logic gates (**3**)	80
5, **6**	EtOH/HEPES (1 mM, pH 7.4, 1 : 1, v/v)	Turn-on	520	582.2	1 : 1 and —	—	0.9 μM (**5**)	Detection in living MGC803 cells (**5**)	81
7	EtOH–H_2O (5/5, v/v, PBS, pH 7.4)	Turn-on	540	581	1 : 1 and 2.99 × 10^6 M^{-1}	Pb^{2+}, Fe^{3+} and Cr^{3+}	0.03 μmol L^{-1}	Detection in L929 mouse fibroblast cells and human osteosarcoma MG-63 cells	82
8	MeOH/H_2O (9 : 1, v/v)	Turn-on	356	554	1 : 1 and —	—	1.45 μM	—	83
9, **10**	MeOH/H_2O, 2 : 1, v/v)	Turn-on	563	583	1 : 1 (**9**) 3 : 2 (probe : metal) (**10**) and 1.57 × 10^4 (**9**) and 1.63 × 10^4 M^{-1} (**10**)	Al^{3+}, Sn^{2+}, Fe^{2+}, Fe^{3+}	2.78 (**9**) and 2.56 μM (**10**)	—	84
11	Acetonitrile	Turn-on	553	583	1 : 1 and —	Zn^{2+}	0.174 nM	—	85
12	EtOH–H_2O, 4 : 1, v/v, HEPES buffer, pH 7.4	Turn-on, PET	344	386, 402	2 : 1 complex (probe : metal) and 2.22 × 10^4 M^{-1}	—	6.93 μM	Detection in living Vero 76 cells	86
13	Water	Turn-on	360	489	1 : 1 and 4.7 × 10^4	Cr^{3+} and Fe^{3+}	4.71 × 10^{-5} M	—	87
14	Water	Turn-on, ICT	374 nm	433, 473	1 : 1 and 1.0 × 10^6 M^{-1}	—	0.268 μM	(a) Discriminative detection in human normal and cancer cells, (b) mitochondria-targeted probe in FaDu cells and (c) real water sample analysis	88
15	DMSO–water (9 : 1,v/v)	Turn-off, ICT	523	585	1 : 1 and —	—	—	Detection in living HeLa cells	89
Sn^{2+} chemosensors									
16	Acetonitrile–HEPES (1 : 4, v/v, 10 mM, pH = 7.4)	Turn-on, TBET	366	442 to 599	1 : 1 and 3.1 × 10^5 M^{-1}	—	5 × 10^{-9} M (5 nM)	Detection in living RAW 264.7 cells	90
17, **18**	Ethanol–water (1 : 1, v/v), pH 7.04.	Turn-on	560	580	1 : 1 and 4.4 × 10^4 (**17**) and 3.8 × 10^4 (**18**)	Cr^{3+}	5.7 × 10^{-7} M (**17**) and 4.6 × 10^{-7} M (**18**)	Detection in eukaryotic (live KB cells) and prokaryotic (live *Streptococcus mutans* cells) cells	91
19	MeOH/H_2O (2 : 3, v/v, pH 5.95)	Turn-on	561	583	1 : 1 and 2.65 × 10^4 M^{-1}	—	0.044 μM	—	92
20	CH_3CN/H_2O (99/1, v/v).	Turn-on	560	577 to 587	1 : 1 and 1.2 × 10^6	—	1.2 × 10^{-7} mol L^{-1} (UV) and 2.6 × 10^{-8} mol L^{-1} (fluorescence)	Determination of Sn^{2+} in synthetic samples	93
21	30% Acetonitrile solution	Turn-on	563	588	1 : 1 and 2.72 × 10^6 M^{-1}	Al^{3+}	5.10 μM	Test kits	94
22	Aqueous solution	Turn-on	280	397	1 : 1 and 5.0 × 10^6 M^{-1}	—	0.115 μM	(a) Detection in zebra fish and human living cells (b) Discriminative identification in human cancer cells and normal cells.	96
23	Buffered aqueous solution	Turn-on, ICT	280	400	1 : 1 and 2.5 × 10^6 M^{-1}	—	79 nM	(a) Detection in live human cells and in zebrafish larvae (b) Discriminative	97

Table 1 (*continued*)

Probe	Solvent	Sensing mechanism	Excitation (nm)	Emission in the presence of the analyte (nm)	Stoichiometry and association constant	Interference	Detection limit	Applications	Ref.
								recognition in human cancer cells and normal living cells	
24	Aqueous solution (20 mM HEPES, pH = 7.5)	Turn-on, PET	276	400	1 : 1 and 1.42×10^6 M^{-1}	Fe^{2+} and Fe^{3+}	4.13×10^{-7} M	(a) Detection in live HaCaT cells and zebrafish (b) Discriminative identification in normal and cancerous human cells	98
25, 26	CH_3CN solution	Turn-on	415	560	—	—	5.44×10^{-6} M (**25**–Hg^{2+}) (from fluorescence)	—	101
27	Methanol	Turn-on	—	454	1 : 2 (metal : probe) and —	—	—	—	102
28	Methanol	Turn-on	310	477	1 : 1 and 4.04×10^3 L mol^{-1}	—	1.9 μM	Detection in several water samples	103
29	DMSO/deionized H_2O (1 : 1, v/v)	Turn-on, PET, CHEF	320	460	1 : 2 and 6.8×10^9 M^{-2}	—	3.14×10^{-7} M	—	105
30	THF solution	Turn-on, ICT	420	561	1 : 1 and 1.6×10^4 M^{-1}	Al^{3+}, Cr^{3+} and Fe^{3+}	0.116 μM	Detection in living HeLa cells	106
31	DMF/H_2O (1 : 1 v/v) solution	Turn-off	322	383 and 571	1 : 2 (probe : metal) and 4.43×10^8 M^{-1}	Co^{2+}	2.21×10^{-9} M	(a) An electronic eye (RGB – Arduino device) and (b) real water sample analysis	108
32	80% aq. DMF solution	Turn-on	425	—	1 : 1 and 4.2×10^5 M^{-1}	Fe^{3+}, Co^{2+}, Hg^{2+}	1.57×10^{-9} M	(a) Hydrogel sensor and RGB sensor device and (b) detection in several water samples	109
33	H_2O : CH_3CN (1 : 1, v/v, pH 7.2, 10 mM Tris–Cl buffer)	Turn-on, PET, CHEF	400	463	1 : 1 and 1.60×10^6 M^{-1}	—	90 nM	Detection in algae samples	110
34	CH_3CN : H_2O (1 : 8, v/v) at pH 7.0 (10 mM phosphate buffer)	Colorimetric, ratiometric	400 to 454	—	1 : 1 and 0.35×10^6 M^{-1}	—	85 nM	Detection in several mouthwash and toothpaste samples	111
35	Acetonitrile	Turn-on	330	582	1 : 1 and $\sim 3.4 \times 10^5$	Al^{3+}	25.7 nM	—	112
36	CH_3CN solution	Turn-on	350	500	1 : 1 and 3.008×10^3 M	Fe^{3+}, Co^{2+}, Ni^{2+} and Cu^{2+}	—	—	113
37	Water	Turn-on, PET	360	415	1 : 1 and 1.48×10^4	Hg^{2+}	—	—	114
38	MeCN : bis–tris buffer (9 : 1, v/v; pH = 7.0) solution	Colorimetric	283	—	2 : 1 and 4.195×10^3 M^{-1}	—	0.754 mol L^{-1}	Test kits	115
39	DMF solution	Turn-on	—	548	—	—	0.168 μM	—	116
40	CH_3CN–H_2O (80/20, v/v)	Turn-on	360 & 378	533	1 : 1 and 7.5×10^5 M^{-1}	Zn^{2+}	8.21×10^{-8} M	Detection in live *Scenedesmus obliquus* cells	117
41	THF– HEPES buffer (90 : 10, v/v, pH 7.4)	Turn-on, CHEF, PET, ESIPT, C=N isomerization	445	488	1 : 1 and 1.50×10^4 M^{-1}	—	0.3898 ppb	—	118
42	Acetone/H_2O (1 : 1) solution	Turn-on	370	560	1 : 1 and —	Al^{3+}	6.31×10^{-8} M	Detection in living A549 cells	119
43	Methanol solution	Turn-on	—	347	1 : 1 and 13.36×10^5 M^{-1}	—	0.47×10^{-7} M(UV) and 3.8×10^{-9} M (fluorescence)	—	120
44	Water	Turn-on	326	339	1 : 1 and 4.19×10^3 M^{-1}	Hg^{2+}, Cr^{3+}, Ni^{2+}, Ba^{2+}	0.5 μM (0.06 ppm)	—	121
45	Mixture of DMSO and 2.0 M HCl (9 : 1, v/v) solution	Colorimetric	353 to 437	—	—	—	5.0×10^{-6} M, 4.8×10^{-6} M (Office scanner)	—	123

constant was determined as 4.19×10^3 M^{-1} using the Benesi–Hildebrand equation (Fig. 12).

2.2.7. Reaction-based chemosensors. Because of their selectivity, sensitivity, and rapid response times, reaction-based

chemosensors (*i.e.*, chemodosimeters) have recently received great attention from researchers.[122] Typically, chemodosimeters use irreversible chemical processes to detect target analytes. In this part, we will look at one example of reaction-based chemosensors.

A reaction-based colorimetric probe **45** was reported by Chang's group and revealed high selectivity to Sn^{2+} over other competitive analytes.[123] The free probe **45** displayed a strong absorption band at 353 nm in a mixed solution (DMSO and 2.0 M HCl, 9 : 1, v/v). In the presence of Sn^{2+}, the absorbance band at 353 nm gradually decreased and a new band with increasing intensity emerged at 437 nm (320-fold). The colorimetric change (from colorless to yellow) in the presence of Sn^{2+} was attributed to the Sn^{2+} induced reduction of the NO_2 group to the amine group. The reduction of the nitro group by Sn^{2+} was confirmed by ^1H NMR spectroscopy and mass spectrometry. A detection limit of 5.0×10^{-6} M for Sn^{2+} was calculated from the UV-vis titration spectra. Using this probe, the authors developed a colorimetric Sn^{2+} ion assay for industrial and laboratory use. Moreover, this probe was also able to produce fluorescence signals in the presence of Sn^{2+}, but this was not very effective because the fluorescence intensity was quite low and noisy (Fig. 13).

3. Conclusion and perspectives

In this review, various research studies emphasizing the development of novel colorimetric and fluorometric sensors (small organic molecule based chemosensors) for tin ions from 2012 to 2022 are presented. Due to the biological and environmental importance of tin ions, there has been a great deal of interest in sensing them. Several fluorophores, including rhodamine, naphthalene, pyrene, coumarin, naphthothiazole, naphthoquinone, diarylethene, triphenylamine and 1,8-naphthalimide, have been combined with various kinds of binding/reaction sites for sensing using various photophysical techniques such as CHEF, PET, ICT, TBET, ESIPT, FRET and C = N isomerization.

The rhodamine derivatives discussed in this study are undoubtedly good candidates (17 chemosensors) for the selective detection of tin ions (Sn^{4+}/Sn^{2+}) among other fluorophores. Generally, for chemosensors based on rhodamine B derivatives, modification was focused on the N-terminus of spiroamide, which was coupled to different moieties for the detection of tin ions.[124] In general, the sensing mechanism of rhodamine-based chemosensors is the reversible ring opening of spirolactam to the amide form in the presence of a metal cation (Sn^{4+}/Sn^{2+}), which causes colour and fluorescence changes. There are several heteroatoms in chemosensors that can be coordinated with tin ions (Sn^{4+}/Sn^{2+}), including imine nitrogen, amide oxygen atoms, phenolic oxygen atoms, and so on. Tin ions, owing to their size, are likely to fit well into this pocket, making these chemosensors selective for the cation.[125]

All of these probes were classified based on their sensing mechanism to different oxidation states of tin. The design approaches, sensing processes, and applications of these fluorescent probes have been discussed here. The majority of the reported tin probes had high selectivity and sensitivity and low detection limits, allowing them to detect tin ions in water samples as well as in living cells. Here, most probes are based on the binding of sensors with tin ions. Most of the sensing processes above are associated with fluorescence and/or colour changes that can be seen with the naked eye. Few authors reported efficient ''test kits'' that can function as ''dip-in'' sensors for the selective and sensitive detection of tin ions. The probes and their sensing mechanisms, stoichiometry and detection limits in various solvents, and applications are presented in Table 1.

Despite the progress in this area, there are also lots of challenges to be addressed.

1. For an excellent chemosensor, selectivity is crucial. In order to detect a specific analyte effectively and accurately, chemosensors should have good selectivity and sensitivity for this analyte to minimise interference from other analytes. Herein, few tin chemosensors are susceptible to interference from other metal cations. As a result, development of new interference-free probes is in high demand.

2. Aqueous solubility is an essential factor for the practical use of chemosensors for various analytes (ions, biomolecules, *etc.*). In this review, it must be noted that most of those chemosensors have been investigated in organic or aqueous media having a large percentage of organic solvents, which prevents their practical applications in complicated environmental and biological systems. One of the main tasks for future research in this area will be the development of chemosensors that can function in totally aqueous media.

3. In terms of sensitivity and selectivity, reaction-based sensing systems, *i.e.*, chemodosimeters, have been identified as potential candidates for colorimetric and fluorometric detection of various analytes. There is only one chemodosimeter reported here. Therefore, further study will be needed to develop more chemodosimeters for the detection of tin ions.

4. All the reported tin-selective probes herein rely on fluorescence intensity measurements (turn-on/turn-off) at a single wavelength, which can be impacted by a variety of external parameters like pH, temperature, instrument efficiency, photobleaching, and unknown analyte concentrations. Ratiometric fluorescent probes, on the other hand, have a wider functionality than intensity-based probes since they enable measurements using the ratio at two different emission wavelengths, which may provide a built-in correction for environmental factors and thus improve the accuracy of detection. Furthermore, development of innovative ratiometric sensors should really be the major direction for future research in this topic.

5. All of the reported chemosensors for Sn^{4+}/Sn^{2+} ions exhibit emission and absorption wavelengths in the visible region. However, both the excitation and emission wavelengths of the probes should be in the near-infrared (NIR, 700–900 nm) region for bioimaging (*in vitro* and *in vivo*) studies, as NIR-probes have benefits over the visible optical response, including longer wavelengths, little tissue injury, extremely low signal interference, and deep tissue penetration. The primary emphasis of

future research in this subject should be the design of NIR-based probes.

6. Although there are some techniques employed in the design and development of fluorescent probes, like metal ion-induced spirolactam ring-opening of the rhodamine moiety, useful and comprehensive ideas are scarce. Hence, continuous efforts should be made to develop novel and inventive fluorometric probes for tin ions.

Prospective research on this topic will include the advancement of fluorogenic probes for tin ions with high selectivity/sensitivity, high miscibility in aqueous systems, large Stokes shifts, high quantum yields, low limits of detection, fast response times, efficient chelation ability, low interference from biological surroundings, photostability, high cell permeability with low cytotoxicity and fluorescence bioimaging capabilities. More and better fluorescent tin sensors are predicted to be developed in the coming years. Finally, we anticipate that this review will provide support in the development of more potent fluorescent probes for a number of different fascinating applications in the future.

Conflicts of interest

There are no conflicts to declare.

References

1 H. Rüdel, *Ecotoxicol. Environ. Saf.*, 2003, **56**, 180–189.
2 Concise International Chemical Assessment Document 65 by WHO, Geneva, 2006.
3 N. Cardarelli, *Thymus*, 1990, **15**, 223–231.
4 J. D. Campbell, *Med. Hypotheses*, 2001, **57**, 521–531.
5 S. G. Schäfer and U. Femfert, *Regul. Toxicol. Pharmacol.*, 1984, **4**, 57–69.
6 L. R. Sherman, J. Masters, R. Peterson and S. Levine, *J. Anal. Toxicol.*, 1986, **10**, 6–9.
7 Y. Arakawa, *Sangyo Eiseigaku Zasshi*, 1997, **39**, 1–20.
8 N. J. Snoeij, A. H. Penninks and W. Seinen, *Environ. Res.*, 1987, **44**, 335–353.
9 J. M. Tsangaris, *Appl. Organomet. Chem.*, 1992, **6**, 3–18.
10 A. M. Florea and D. Büsselber, *Biometals*, 2006, **19**, 419–427.
11 C. M. Viau, T. N. Guecheva, F. G. Sousa, C. Pungartnik, M. Brendel, J. Saffi and J. A. P. Henriques, *Arch. Toxicol.*, 2009, **83**, 769–775.
12 E. Rojas, L. A. Herrera, L. A. Poirier and W. P. Ostrosky, *Mutat. Res.*, 1999, **443**, 157–181.
13 S. G. Schafer and U. Femfert, *Regul. Toxicol. Pharmacol.*, 1984, **4**, 57–69.
14 E. J. Bulten and H. A. Meinema, Tin, in *Metals and their compounds in the environment: Occurrence, analysis, and biological relevance*, ed. E. Merian, VCH, Weinheim, 1991, pp. 1243–1259.
15 J. Stellman, *The ILO Encyclopaedia of Occupational Health and Safety: a multidisciplinary challenge*, International Labour Office, Geneva, 1998, vol. 137, no. 3.
16 A. L. Cardoso, S. C. Gonzaga Neves and M. J. da Silva, *Energies*, 2008, **1**, 79–92.
17 X. H. Tan, B. Shen, L. Liu and Q. X. Guo, *Tetrahedron Lett.*, 2002, **43**, 9373–9376.
18 M. Hamberg and B. Samuelsson, *Proc. Natl. Acad. Sci. U. S. A.*, 1973, **70**, 899–903.
19 F. Li, J. Song, H. Yang, S. Gan, Q. Zhang, D. Han, A. Ivaska and L. Niu, *Nanotechnology*, 2009, **20**, 1–5.
20 C. S. Cho, H. K. Lim, S. C. Shim, T. J. Kim and H. J. Choi, *Chem. Commun.*, 1998, 995–996.
21 K. K. Upadhyay, R. K. Mishra and A. Kumar, *Catal. Lett.*, 2008, **121**, 118–120.
22 M. Hoch, *Appl. Geochem.*, 2001, **16**, 719–743.
23 C. I. Yoo, Y. Kim, K. S. Seong, C. S. Sim, N. Choy, J. Kim, J. B. Eum, Y. Nakajima, Y. Endo and Y. J. Kim, *J. Occup. Health*, 2007, **49**, 305–310.
24 A. C. A. Sousa, M. R. Pastorinho, S. Takahashi and S. Tanabe, *Environ. Chem. Lett.*, 2014, **12**, 117–137.
25 K. Fent, *Crit. Rev. Toxicol.*, 1996, **26**, 1–117.
26 N. Tinanoff, *Int. J. Clin. Dent.*, 1995, **6**, 37–40.
27 H. J. Keene, I. L. Shklair and G. J. Mickel, *J. Dent. Res.*, 1977, **56**, 21.
28 H. J. Keene, I. L. Shklair, G. J. Mickel and M. R. Wirthlin, *J. Dent. Res.*, 1977, **56**, 5–10.
29 A. C. S. Braga, M. B. N. Oliveira, G. D. Feliciano, I. W. Reiniger, J. F. Oliveira, C. R. Silva and M. Bernardo, *Curr. Pharm. Des.*, 2000, **6**, 1179–1191.
30 M. L. B. Assis, J. B. C. Neto, J. E. Q. Souza, A. Caldeira-de-Araújo and M. Bernardo-Filho, *Cancer Lett.*, 1998, **130**, 127–131.
31 Z. Lei, *Chin. Sci. Bull.*, 2005, **50**, 2390–2392.
32 Agency for Toxic substances and Disease Registry (ATSDR), 2005.
33 A. Tomza-Marciniak, B. Pilarczyk, A. Marciniak, R. Pilarczyk and M. Bakowska, Tin, Sn, in *Mammals and Birds as Bioindicators of Trace Element Contaminations in Terrestrial Environments*, ed. E. Kalisińska, Springer, Cham, Switzerland, 2019.
34 K. A. Winship, *Adverse Drug React. Acute Poisoning Rev.*, 1988, **7**, 19–38.
35 C. J. Benoy, P. A. Hooper and R. Schneider, *Food Cosmet. Toxicol.*, 1971, **9**, 645–654.
36 M. A. Ghaffari and B. Motlagh, *Iran. Biomed. J.*, 2011, **15**, 38–43.
37 E. Boniewska-Bernacka, D. Man, R. Slota and M. A. Broda, *J. Biochem. Mol. Toxicol.*, 2011, **25**, 231–237.
38 B. Michalke, S. Halbach and V. Nischwitz, *J. Environ. Monit.*, 2009, **11**, 939–954.
39 D. Ghazi, Z. Rasheed and E. Yousif, *International Journal of Research in Engineering and Innovation*, 2018, **2**, 340–348.
40 M. Aschner and J. L. Aschner, *Neurosci. Biobehav. Rev.*, 1992, **16**, 427–435.
41 T. Guérin, V. Sirot, J.-L. Volatier and J.-C. Leblanc, *Sci. Total Environ.*, 2007, **388**, 66–77.
42 W. T. Piver, *Environ. Health Perspect.*, 1973, **4**, 61–79.

43 World Health Organization & International Programme on Chemical Safety, *Tin and organotin compounds a preliminary review*, World Health Organization, Geneva, 1980, https://apps.who.int/iris/handle/10665/39658.
44 A. O. Sunday, B. A. Alafara and O. G. Oladele, *Chem. Speciation Bioavailability*, 2012, **24**, 216–226.
45 E. Dopp, A. W. Rettenmeier, R. H. Kretsinger and V. N. Uversky, in *Encyclopedia of Metalloproteins*, ed. E. A. Permyakov, Springer, New York, 2013.
46 S. Blunden and T. Wallace, *Food Chem. Toxicol.*, 2003, **41**, 1651–1662.
47 Codex Alimentarius Commission, Procedural Manual, Foods and Agriculture Organization of the UN/World Health Organization, Rome 2001.
48 R. E. Sturgeon, S. N. Willie and S. S. Berman, *Anal. Chem.*, 1987, **59**, 2441–2444.
49 F. Heppeler, S. Sander and G. Henze, *Anal. Chim. Acta*, 1996, **319**, 19–24.
50 S. Ichinoki, H. Iwase, F. Arakawa, K. Hirano and Y. Fujii, *J. Liq. Chromatogr. Relat. Technol.*, 2003, **26**, 3129–3139.
51 Z. P. Yang, M. Alafandy, K. Boutakhrit, J. M. Kauffmann and J. Arcos, *Electroanalysis*, 2005, **8**, 25–29.
52 S. Ulusoy, H. I. Ulusoy and M. Akcay, *Food Chem.*, 2012, **134**, 419–426.
53 I. A. Ismail and A. M. El-Kot, *Microchem. J.*, 1991, **44**, 49–53.
54 M. Arvand, A. M. Moghimi, A. Afshari and N. Mahmoodi, *Anal. Chim. Acta*, 2006, **579**, 102–108.
55 K. Agarwal, K. S. Patel, K. Shrivas, V. K. Jain and F. Khan, *J. Hazard. Mater.*, 2009, **164**, 95–98.
56 A. S. Dadda, A. C. Teixeira, P. K. Feltes, M. M. Campos, C. E. Leite and C. M. Moriguchi-Jeckel, *J. Braz. Chem. Soc.*, 2014, **25**, 1621–1629.
57 S. Rubio, A. Gomez-Hens and M. Valcarcel, *Analyst*, 1985, **110**, 43–45.
58 A. A. Ribeiro, A. L. Moretto, M. A. Z. Arruda and S. Cadore, *Microchim. Acta*, 2003, **141**, 149–155.
59 S. K. Samanta, K. Maiti, S. K. Manna, S. S. Ali, U. N. Guria, A. Ghosh, P. Datta and A. K. Mahapatra, *Dyes Pigm.*, 2021, **196**, 109758.
60 A. Maiti, S. K. Manna, D. Banik and A. K. Mahapatra, *New J. Chem.*, 2021, **45**, 20046–20074.
61 S. K. Manna, T. K. Achar and S. Mondal, *Anal. Methods*, 2021, **13**, 1084–1105.
62 D. Banik, S. K. Manna and A. K. Mahapatra, *Spectrochim. Acta, Part A*, 2021, **246**, 119047.
63 S. K. Manna, A. Gangopadhyay, K. Maiti, S. Mondal and A. K. Mahapatra, *ChemistrySelect*, 2019, **4**, 7219–7245.
64 B. Kaur, N. Kaur and S. Kumar, *Coord. Chem. Rev.*, 2018, **358**, 13–69.
65 H.-H. Han, H. Tian, Jr., Y. Zang, A. C. Sedgwick, J. Li, J. L. Sessler, X.-P. He and T. D. James, *Chem. Soc. Rev.*, 2021, **50**, 9391–9429.
66 Z. Liu, W. He and Z. Guo, *Chem. Soc. Rev.*, 2013, **42**, 1568–1600.
67 J. Fan, M. Hu, P. Zhan and X. Peng, *Chem. Soc. Rev.*, 2013, **42**, 29–43.
68 J. Wu, W. Liu, J. Ge, H. Zhang and P. Wang, *Chem. Soc. Rev.*, 2011, **40**, 3483–3495.
69 S. Das, M. Dutta and D. Das, *Anal. Methods*, 2013, **5**, 6262–6285.
70 J. Krämer, R. Kang, L. M. Grimm, L. D. C. P. Picchetti and F. Biedermann, *Chem. Rev.*, 2022, **122**, 3459–3636.
71 J.-T. Hou, N. Kwon, S. Wang, B. Wang, X. He, J. Yoon and J. Shen, *Coord. Chem. Rev.*, 2022, **450**, 214232.
72 S. K. Sahoo, *New J. Chem.*, 2021, **45**, 8874–8897.
73 P. Mahato, S. Saha, P. Das, H. Agarwalla and A. Das, *RSC Adv.*, 2014, **4**, 36140–36174.
74 H. A. Anila, F. Ali and A. Das, *Compr. Supramol. Chem. II*, 2017, **8**, 319–349.
75 H. Singh, K. Tiwari, R. Tiwari, S. K. Pramanik and A. Das, *Chem. Rev.*, 2019, **119**, 11718–11760.
76 H. N. Kim, M. H. Lee, H. J. Kim, J. S. Kim and J. Yoon, *Chem. Soc. Rev.*, 2008, **37**, 1465–1472.
77 Q. Zhang and K. M.-C. Wong, *Coord. Chem. Rev.*, 2020, **416**, 213336.
78 Q. Wang, C. Li, Y. Zou, H. Wang, T. Yi and C. Huang, *Org. Biomol. Chem.*, 2012, **10**, 6740–6746.
79 A. K. Mahapatra, S. K. Manna, D. Mandal and C. D. Mukhopadhyay, *Inorg. Chem.*, 2013, **52**, 10825–10834.
80 A. K. Mahapatra, S. K. Manna, K. Maiti, R. Maji, C. D. Mukhopadhyay, D. Sarkar and T. K. Mondal, *RSC Adv.*, 2014, **4**, 36615–36622.
81 J. Cheng, E. Yang, P. Ding, J. Tang, D. Zhang, Y. Zhao and Y. Ye, *Sens. Actuators, B*, 2015, **221**, 688–693.
82 Z. Yang, M. She, S. Ma, B. Yin, P. Liu, X. Liu, S. Zhao and J. Li, *Sens. Actuators, B*, 2017, **242**, 872–879.
83 X. Wang, L. Zhang, S. Zhuang, M. Huang and Y. Gao, *Appl. Organomet. Chem.*, 2019, **33**, e5067.
84 L. Brulíkova, T. Volná and J. Hlavac, *ACS Omega*, 2020, **5**, 9324–9333.
85 K. R. Chethana, K. Sureshkumar, S. Muralikrishna and T. Ramakrishnappa, *Mater. Today: Proc.*, 2022, **49**, 620–627.
86 A. K. Mahapatra, S. Mondal, K. Maiti, S. K. Manna, R. Maji, D. Mandal, S. Mandal, S. Goswami, C. K. Quah and H.-K. Fun, *RSC Adv.*, 2014, **4**, 56605–56614.
87 J. Liu, K. Wu, X. Li, Y. Han and M. Xia, *RSC Adv.*, 2013, **3**, 8924–8928.
88 P. Ravichandiran, D. S. Prabakaran, N. Maroli, A. R. Kim, B.-H. Park, M.-K. Han, T. Ramesh, S. Ponpandian and D. J. Yoo, *J. Hazard. Mater.*, 2021, **419**, 126409.
89 L. Zhu, J. Yang, Q. Wang and L. Zeng, *J. Lumin.*, 2014, **48**, 161–164.
90 S. Adhikari, A. Ghosh, S. Guria and A. Sahana, *RSC Adv.*, 2016, **6**, 39657–39662.
91 H. Lan, Y. Wen, Y. Shi, K. Liu, Y. Mao and T. Yi, *Analyst*, 2014, **139**, 5223–5229.
92 X. Bao, X. Cao, X. Nie, Y. Jin and B. Zhou, *Molecules*, 2014, **19**, 7817–7831.
93 Z. Yan, G. Wei, S. Guang, M. Xu, X. Ren, R. Wu, G. Zhao, F. Ke and H. Xu, *Dyes Pigm.*, 2018, **159**, 542–550.
94 P. W. Cheah, M. P. Heng, A. Izati, C. H. Ng and K. W. Tan, *Inorg. Chim. Acta*, 2020, **512**, 119901.

95 M. Janeczko, O. M. Demchuk, D. Strzelecka, K. Kubiński and M. Masłyk, *Eur. J. Med. Chem.*, 2016, **124**, 1019–1025.
96 P. Ravichandiran, V. K. Kaliannagounder, A. P. Bella, A. Boguszewska-Czubara, M. Masłyk, C. S. Kim, C. H. Park, P. M. Johnson, B.-H. Park, M.-K. Han, A. R. Kim and D. J. Yoo, *Anal. Chem.*, 2021, **93**, 801–811.
97 P. Ravichandiran, D. S. Prabakaran, N. Maroli, A. Boguszewska-Czubara, M. Masłyk, A. R. Kim, P. Kolandaivel, P. Ramalingam, B.-H. Park, M.-K. Han, T. Ramesh and D. J. Yoo, *J. Hazard. Mater.*, 2021, **415**, 125593.
98 P. Ravichandiran, D. S. Prabakaran, A. P. Bella, A. Boguszewska-Czubara, M. Maslyk, K. Dineshkumar, P. M. Johnson, B.-H. Park, M.-K. Han, H. G. Kim and D. J. Yoo, *ACS Sustainable Chem. Eng.*, 2020, **8**, 10947–10958.
99 L. Zhai, Y. Tu, Z. Shi and S. Pu, *Spectrochim. Acta, Part A*, 2019, **218**, 171–177.
100 H. Tian and S. Yang, *Chem. Soc. Rev.*, 2004, **33**, 85–97.
101 S. Liu, S. Tan, H. Hu, Z. Chen and S. Pu, *J. Photochem. Photobiol., A*, 2021, **418**, 113439.
102 S. Pu, Y. Xu, C. Zheng, W. Geng, S. Cui and G. Liu, *Tetrahedron*, 2014, **70**, 9070–9076.
103 S. Qu, C. Zheng, G. Liao, C. Fan, G. Liu and S. Pu, *RSC Adv.*, 2017, **7**, 9833–9839.
104 A. Karak, S. K. Manna and A. K. Mahapatra, *Anal. Methods*, 2022, **14**, 972–1005.
105 F. Kolcu, D. Erdener and I. Kaya, *Synth. Met.*, 2021, **272**, 116668.
106 X. Meng, L. You, S. Li, Q. Sun, X. Luo, H. He, J. Wang and F. Zhao, *RSC Adv.*, 2020, **10**, 37735–37742.
107 E. C. Constable, *Chem. Soc. Rev.*, 2007, **36**, 246–253.
108 R. Manivannan, J. Ryu and Y.-A. Son, *Dyes Pigm.*, 2021, **192**, 109425.
109 G. Heo, R. Manivannan, H. Kim, M. J. Kim, K. S. Min and Y.-A. Son, *Sens. Actuators, B*, 2019, **297**, 126723.
110 S. Saha, S. Kamila, A. Chattopadhyay and P. Sahoo, *New J. Chem.*, 2022, **46**, 4233–4238.
111 S. Kundu, K.-N. Truong, S. Saha, K. Rissanen and P. Sahoo, *Sci. Rep.*, 2022, **12**, 2305.
112 S. Adhikari, S. Mandal, A. Ghosh, S. Guria and D. Das, *Dalton Trans.*, 2015, **44**, 14388–14393.
113 S. Prabhu, S. Saravanamoorthy, M. Ashok and S. Velmathi, *J. Lumin.*, 2012, **132**, 979–986.
114 D. Udhayakumari, S. Suganya and S. Velmathi, *J. Lumin.*, 2013, **141**, 48–52.
115 P. R. Dongare, A. H. Gore and B. D. Ajalkar, *Inorg. Chim. Acta*, 2020, **502**, 119372.
116 X.-L. Ye, P. Li, Y.-L. Liu, X.-M. Liang and L. Yang, *Inorg. Chem. Commun.*, 2021, **130**, 108739.
117 M. Z. Jonaghani, H. Zali-Boeini, R. Taheri, H. A. Rudbaria and B. Askaria, *RSC Adv.*, 2016, **6**, 34940–34945.
118 A. G. Jadhav, S. S. Shinde, S. K. Lanke and N. Sekar, *Spectrochim. Acta, Part A*, 2017, **174**, 291–296.
119 A. Gul, M. Oguz, A. N. Kursunlu and M. Yilmaz, *Dyes Pigm.*, 2020, **176**, 108221.
120 G. Singh, P. Sushma, P. Mohit, P. Satija, M. A. Esteban, D. Gonzalez-Silvera and C. Espinosa-Ruiz, *ChemistrySelect*, 2021, **6**, 7613–7621.
121 W. Jianqiang, L. Mengyuan, W. Zhiwei, Z. Man, G. Changqing and G. Cheng, *J. Photochem. Photobiol., A*, 2015, **309**, 37–46.
122 Y. Yang, Q. Zhao, W. Feng and F. Li, *Chem. Rev.*, 2013, **113**, 192–270.
123 J. H. Baek, M. G. Choi, N. Y. Kim and S.-K. Chang, *Sens. Actuators, B*, 2019, **284**, 562–567.
124 X. Chen, T. Pradhan, F. Wang, J. S. Kim and J. Yoon, *Chem. Rev.*, 2012, **112**, 1910–1956.
125 P. Roy, *Dalton Trans.*, 2021, **50**, 7156–7165.

